

MULTI-FUNCTIONAL SYSTEM FOR BIOMEDICAL
APPLICATION USING AC ELECTROKINETICS

A Thesis

by

RAKESH GUDURU

Submitted to the Graduate College of
The University of Texas Rio Grande Valley
In partial fulfillment of the requirements for the degree of
MASTER OF SCIENCE ENGINEERING

August 2017

Major Subject: Electrical Engineering

MULTI-FUNCTIONAL SYSTEM FOR BIOMEDICAL
APPLICATION USING AC ELECTROKINETICS

A Thesis
by
RAKESH GUDURU

COMMITTEE MEMBERS

Dr. Nazmul Islam
Committee Chair

Dr. Sanjeev Kumar
Committee Member

Dr. Yoonsu Choi
Committee Member

August 2017

Copyright 2017 Rakesh Guduru

All Rights Reserved

ABSTRACT

Guduru, Rakesh, Multi-Functional System for Biomedical Application using AC Electrokinetics.

Master of Science in Engineering (MSE), August 2017, 60 pp, 3 tables, 18 figures, references, 64 titles.

Manipulation of fluids in a small volume is often a challenge in the field of Microfluidics. While many research groups have addressed this issue with robust methodologies, manipulating fluids remains a scope of study due to the ever-changing technology (Processing Tools) and increase in the demand for “Lab-On-a-Chip” devices in biological applications. This thesis peruses the flow pattern of the orthogonal electrode pattern and circular electrode providing, examples of the flow patterns and the process micromixing. Characteristics of a multifunctional system were demonstrated using orthogonal electrode and circular electrode patterned device. Conductivity of the fluids were chosen such they reflect perfect biological conditions to determine the working conditions of the proposed devices under different AC voltage and frequency levels. Experimental results were then compared with simulated results which were obtained using COMSOL simulation software.

DEDICATION

I would like to dedicate my thesis to my parents, grandparents, and friends for their financial, moral and continuous support.

ACKNOWLEDGMENTS

I would first like to thank my thesis advisor Dr. Nazmul Islam. I thank him for keeping me in place emotionally, whenever I ran into a trouble spot or had a question about my research or writing. He consistently allowed this paper to be my own work, but steered me in the right the direction whenever he thought I needed it.

I would also like to acknowledge Dr. Sanjeev Kumar and Dr. Yoonsu Choi, for being the committee members of this thesis, and I am gratefully indebted to their very valuable comments on this thesis.

Finally, I must express my profound gratitude to my parents and to my friends for providing me with unfailing support and continuous encouragement throughout my years of study and through the process of researching and writing this thesis. This accomplishment would not have been possible without them. Thank you.

TABLE OF CONTENTS

	Page
ABSTRACT	iii
DEDICATION.....	iv
ACKNOWLEDGMENTS	v
TABLE OF CONTENTS	vi
LIST OF TABLES	viii
LIST OF FIGURES	ix
CHAPTER I. INTRODUCTION.....	1
1.1 Microfluidics: Past, Present and Future.....	1
1.2 Electrokinetics.....	2
1.3 AC Electrokinetics-Basic Theory.....	2
1.3.1 Dielectrophoresis (DEP).....	3
1.3.2 AC Electroosmosis (ACEO).....	4
1.3.3 AC Electrothermal effect (ACET)	7
1.4 Micropumps	10
1.5 Micromixers	12
CHAPTER II LITERATURE REVIEW.....	14
2.1 ACEO & ACET Micropumping	14
2.2 Micromixing.....	20
2.3 Particle Manipulation	24

CHAPTER III. DEVICE FABRICATION	25
3.1 Properties of PDMS	25
3.1.1 Mechanical Properties of PDMS	26
3.2 Fabrication Process of Orthogonal Electrode	28
3.3 Fabrication Process of Circular Electrode Pattern	29
CHAPTER IV. ANALYSIS AND SIMULATION	31
4.1 COMSOL for Microfluidics	31
4.2 Micro PIV System	32
4.3 Experimental Procedure for Orthogonal Electrodes	34
4.4 Numerical Analysis of Circular Electrode Pair	34
CHAPTER V. RESULTS AND DISCUSSION	37
5.1 Orthogonal Electrode Pattern	37
5.1.1 Micro-Pumping	38
5.1.2 Micro-Mixing	40
5.1.3 Bio/Nano Particle Trapping	41
5.1.4 Comparison with the Previous Work	42
5.2 Circular Electrode Pattern	42
5.2.1 Comparison Between the Experimental and Simulated Results	47
5.2.2 Micromixing efficiency	51
CHAPTER VI. CONCLUSION AND FUTURE SCOPE	53
REFERENCES	54
BIOGRAPHICAL SKETCH	60

LIST OF TABLES

	Page
Table 1: Properties of PDMS.....	27
Table 2: Observed frequency range for the pumping of the three fluids with different conductivities at 15V _{pp}	39
Table 3: Values of τ and f_c for fluid conductivities 0.073 S/m & 1.62 S/m	45

LIST OF FIGURES

	Page
Figure 1: Electric field distribution showing four counter-rotating vortices above a pair of coplanar electrode.....	15
Figure 2a: Simulation of net flow produced by ACET over two electrodes of different widths. [13] The design of electrode array and power applied setup	17
Figure 2b: Pumping by T electrode at 14 Vrms, 1 MHz. [13].....	18
Figure 3: Different actuation configurations of side electrode arrays. (a) Two opposing arrays (Side1), (b) two sidelong arrays (Side2), (c) three arrays (Side3), (d) all side arrays (Side4), and (e) conventional single array (Side5). The fluidic channel has a hydraulic diameter of 300 μm and the substrate thickness is 200 μm . [20].....	23
Figure 4: Sylgard 184 silicone elastomer base and curing agent	26
Figure 5: Laurell WS-650-15B Spin Coater	29
Figure 6: Orthogonal electrode pair on a PDMS coated glass slide.	29
Figure 7: Circular electrode pair device with cross-sectional view	30
Figure 8: Micro PIV system	33
Figure 9a: Simulated geometrical model in FEMLAB-COMSOL Multiphysics.....	35
Figure 9b: A cross-sectional view of COMSOL simulated electrical potential distribution in the Circular electrode pair	35
Figure 10: Simulation results for fluid conductivity $\sigma=1.632 \text{ S/m}$ at 5V, 800kHz	36
Figure 11a: Maximum velocity plot at 6Vpp representing a bell shape from 10 kHz to 50 kHz.....	38
Figure 11b: Experimental results representing the maximum velocity at 20Vpp at a frequency range of 500Hz to 1.2MHz	38
Figure 12: The figure shows the pumping action of the fluid (PBS) at 80Khz and 15Vpp obtained from Tecplot Focus software	40

Figure 13: Experimental results show the formation of vortices at 100KHz 15Vpp obtained from micro-PIV Tecplot.....	41
Figure 14a: Graphical representation of fluid velocities at 50kHz, 500kHz and 1MHz with applied voltage varying from 1Vpp to 7Vpp, $\sigma=1.632$ S/m.....	43
Figure 14b: Graphical representation of fluid velocities at 50kHz, 500kHz and 1MHz with applied voltage varying from 1Vpp to 7Vpp, $\sigma =0.073$ S/m	44
Figure 15a: Peak velocity of the fluid (conductivity = 1.632S/m) at 5Vpp with frequency ranging from 100kHz to 1MHz.....	46
Figure 15b: Peak velocity of the fluid (conductivity = 0.073S/m) at 5Vpp with frequency ranging from 100kHz to 1.5 MHz.....	46
Figure 16: Generation of chaotic flow at 5Vpp, 600kHz with fluid conductivity 1.632 S/m.....	47
Figure 17a: Disparity between the experimental and simulated results obtained on the fluid with conductivity 1.62 S/m at 1 MHz and different voltage levels.	48
Figure 17b: Disparity between the experimental and simulated results obtained on the fluid with conductivity 1.62 S/m at 500 kHz and different voltage levels.....	48
Figure 17c: Disparity between the experimental and simulated results obtained on the fluid with conductivity 1.62 S/m at 50 kHz and different voltage levels	49
Figure 18a: Disparity between the experimental and simulated results obtained on the fluid with conductivity 0.073 S/m at 1 MHz and different voltage levels	50
Figure 18b: Disparity between the experimental and simulated results obtained on the fluid with conductivity 0.073 S/m at 500 kHz and different voltage levels.....	50
Figure 18c: Disparity between the experimental and simulated results obtained on the fluid with conductivity 0.073 S/m at 50 kHz and different voltage levels.....	51

CHAPTER I

INTRODUCTION

1.1 Microfluidics: Past, Present and Future

Microfluidics exploits the behavior of fluids in microchannels. As the dimensions of the microchannels are often in millimeters or nanometers, the amount of the fluid flowing through the microchannel would be in microliters (10^{-6}) or even down to picoliters (10^{-12}). Not to mention that one drop of fluid or liquid is equal to 50 microliters. Lab-on-a-Chip (LOC) also referred as micro-Total Analysis System (μ TAS) may use microfluidics to carry out various functions like pumping, particle separation, fluid mixing and particle detection to list a few. LOC have become more common in biological and biochemical applications making research groups to come up with a new approach for every problem there is to face with the existing techniques. And also, with the advantages like; small size, high sensitivity and accuracy, low power consumption and short time analysis LOC have begun to enjoy persistent attention by many academic research groups since the past few years.

In this work implementation of microfluidics technologies namely pumping and mixing using AC Electrokinetic (AC EK) techniques were presented with two different electrode arrangements. The following section contains a brief explanation of micropumps and micromixers.

1.2 Electrokinetics

AC electrokinetics is one the enthralling research area due to its applications in different fields of microfluidics. Lab-on-a-chip (LOC) or micro-total analysis systems (μ TAS) have become more common in biological and biochemical applications making research groups to come up with a new approach for every problem there is to face with the existing techniques. The objective of this chapter is to provide an insight on the previous research techniques involved in the manipulation of fluids using AC Electrokinetics.

Electrokinetics forces can be actuated by DC or AC electric signals however; DC EK requires high voltages which can cause electrochemical reactions between the electrode and electrolyte. Also, application of high voltages may come with the side-effects like generation of bubbles and *pH* gradients. Overcoming these potential backdrops, AC EK techniques have been adopted from 1970's. Some of the advantages of ACEK include low operating voltages, various manipulation methods, low power consumption and the ease of fabrication. The following section presents a brief description of the AC EK techniques.

1.3 AC Electrokinetics – Basic Theory

AC Electrokinetics (AC EK) refers to the induced fluid motion due to the external application of AC electric fields. AC EK is classified into three broad areas; dielectrophoresis (DEP), AC electrothermal flow (ACET), and AC electro-osmosis (ACEO). ACEK forces can be actuated by DC or AC electric signals however; DC EK requires high voltages which can cause electrochemical reactions between the electrode and electrolyte. Also, application of high voltages may come with the side-effects like generation of bubbles and *pH* gradients. Overcoming these potential backdrops, AC EK techniques have been adopted from 1970's. Some of the advantages of ACEK include low operating voltages, various manipulation methods,

low power consumption and the ease of fabrication. Details of the three forces are explained in the following section.

1.3.1 Dielectrophoresis (DEP):

When a particle is subjected to a non-uniform external electric field it experiences a net force and moves in the direction of either high electric field strength or low electric field strength due to the polarity difference between the particle and the surrounding medium, this causes DEP. If a suspended particle has polarizability higher than the medium, the DEP force will push the particle toward regions of higher electric field (positive DEP). If the medium has a higher polarizability than the suspended particle, the particle is driven toward regions of low field strength (negative DEP). Factors such as applied electric field, size of the particle, conductivity and permittivity of the media and the particle subjected to the electric field also play a prominent role to change the direction and magnitude of the forces. DEP can be applied in medical diagnostics, drug discovery, cell therapy, and bio-threat defense to name a few.

The force exerted on the particle by DEP is given by the equation:

$$F_{DEP} = \pi \epsilon a^3 \operatorname{Re} \left[\frac{\tilde{\epsilon}_p - \tilde{\epsilon}_m}{\tilde{\epsilon}_p + 2\tilde{\epsilon}_m} \right] \nabla |E|^2 \quad (\text{Eq 1})$$

$\tilde{\epsilon}_p$ is permittivity of the particles and $\tilde{\epsilon}_m$ is the permittivity of the medium.

$$\tilde{\epsilon}_{p,m} = \epsilon_{p,m} - i \left(\frac{\sigma_{p,m}}{\omega} \right) \quad (\text{Eq 2})$$

$\sigma_{p,m}$ is the electrical conductivity of the particle and medium respectively, a is the particle diameter, η is the fluid viscosity. The parameter $\left[\frac{\tilde{\epsilon}_p - \tilde{\epsilon}_m}{\tilde{\epsilon}_p + 2\tilde{\epsilon}_m} \right]$ is known as Clausius

Mossotti (CM) factor. CM factor can be described as a criterion that describes how the effective

movement of the particles varies by changing the material properties and the applied frequency. As CM factor is the function of complex permittivity of the particle and the suspending medium varying between -0.5 and 1, it can also determine the direction of the particle. It should be noted that the spatial dependence of the DEP forces comes from the gradient of the electric field squared DEP is strong only near the electrodes. As the experiments in this thesis had larger electrode gaps DEP force is neglected.

1.3.2 AC Electroosmosis(ACEO):

The surface of the electrode immersed in an electrolyte consists of negative charges which tend to attract the positive charges present in the ionic liquid. The strong bond between the positive charge and negative charge creates an immobile layer known as stern layer. A net positive charge is created above the stern layer due to the attraction between positive and negative charges; this region with net positive charge is known as electrical double layer (EDL). The electrical potential present at the stern layer is known as Zeta (ζ) potential. The length scale at which the zeta potential reduces to zero in the fluid bulk is called Debye length [3]. Debye length is usually in the order of 10nm. When an electrical potential is applied to the electrodes present in the solution, the counter-ions present in the solution are electrostatically attracted to the electrodes, and the opposite polarity charges get attracted towards the excitation voltage. This polarization process can be termed as capacitive charging. The capacitive charging present in the electrical double layer experiences a force due to the interaction with the tangential field thus creating a microflow or AC Electroosmotic (ACEO) Flow.

The electric potential, ϕ , is related to the net charge density through Poisson's equation:

$$\nabla^2\phi = -\frac{\rho}{\epsilon} \quad (\text{Eq 3})$$

Since the thickness is very small when compared to the height of the microchannel, the net charge that occur within the double layer are negligible when compared to the net neutral charge that exists in the bulk of the fluid. Therefore, considering the domain to be charge neutral, the net charge density is assumed to be zero. Thus, the governing equation in the domain becomes:

$$\nabla^2 \phi = 0 \quad (\text{Eq 4})$$

The potential at the electrode-fluid interface is calculated using the following equation:

$$\sigma n \nabla \phi_{DL} = \frac{\phi_{DL} - V_{applied}}{Z_{DL}} \quad (\text{Eq 5})$$

Corresponding equations:

$$\text{Double layer Impedance: } Z_{DL} = \frac{1}{i\omega C_{DL}} \quad (\text{Eq 6})$$

$$\text{Double layer Capacitance: } C_{DL} = \frac{\varepsilon}{\lambda_{Debye}} \quad (\text{Eq 7})$$

where σ is the electric conductivity of the fluid, ε is the electric permittivity of the fluid, ϕ_{DL} is the potential at the outer edge of the EDL, n is the vector normal to the surface, λ_{Debye} is the height of the Gouy–Chapman layer of the EDL and i is the imaginary part.

As, the concept of the ACEO pump is to drive a fluid by means of Electroosmosis, there is no pressure difference imposed on the fluid in order to drive the fluid flow. Therefore, an equation must be used to find the fluid flow over the electrodes. Since the microchannel height is several orders of magnitude larger than the Debye length, the fluid velocity that is created by the EDL can be imposed on the electrode-fluid interface rather than the shear plane created at the interface of the different layers of the EDL. The Helmholtz–Smoluchowski formula characterizes the fluid flow over the electrode:

$$u_{slip} = -\frac{\varepsilon}{\eta} \Delta \phi_d \frac{\partial \phi}{\partial x} = \frac{\varepsilon}{\eta} \Delta \phi_d E_x \quad (\text{Eq 8})$$

By neglecting the initial terms, time-average component of the velocity can be calculated. This is favorable since the only component of the velocity that can be measured experimentally is the time-averaged velocity. Using this assumption yields a time-averaged slip velocity imposed at the fluid-solid interface:

$$\{u_{slip}\} = \frac{\varepsilon}{2 \cdot \eta} \Delta \cdot \Delta \phi_d E_x \quad (\text{Eq 9})$$

where $E_x = -\frac{\partial \phi}{\partial x}$ is the tangential electric field just outside the diffuse layer and $\Delta \phi_d = \phi - \psi$ is the difference between the potential, ϕ , on the outer side of the diffuse layer and ψ , is at inner side of the diffuse layer, at the nonslip plane. ψ becomes the zeta potential, ζ , which is the potential at the interface of the Stern and Gouy–Chapman Layers that categorizes the EDL. Again, the height of the channel is larger than the Debye length, resulting in the zeta potential becoming ψ . The zeta potential, ζ , is a difficult variable to approximate due to the variations in the creation of the Stern Layer. For accurate values, the zeta potential should be measured experimentally and should be dependent on the type of fluid chosen, the fluid's electric conductivity, the type of electrolyte that is diffused into the fluid, the solid surface the fluid interacts with, and the frequency of excitation and voltage. In the current application, the top and bottom of the microchannel or perfusion chamber have boundaries set to no-slip boundary conditions and the side walls are set to open boundary conditions.

To solve for the fluid flow induced in the microchannel, the incompressible Navier–Stokes equation is discussed in the AC electrothermal governing equations.

In general, ACEO fluid velocity is given by the following equation:

$$u_{ACEO} = -\left(\frac{\varepsilon_m}{\eta}\right) \cdot \Delta \xi \cdot E \quad (\text{Eq 10})$$

Where η and ε_m are the viscosity and permittivity of the medium, E is the tangential electric field and voltage drop over the EDL is denoted by $\Delta\xi$. In this equation η and ε_m can be considered as constant. Fluid velocity due to ACEO is has a linear dependence on the applied voltage and frequency. Many research groups believe that the force due to the ACEO is negligible if the applied frequency is higher (>100 kHz is most of the cases) as it's range of operation is 100 Hz to 100 kHz due it's dependency on frequency having an optimal frequency range of 1kHz-10kHz to achieve maximum velocity therefore, posing a risk of zero induced net fluid velocity if the conductivity of the electrolyte increases. As, Biomedical fluids frequently involve conductivity higher than 10^{-2} S m^{-1} , majority of the research groups started working on developing ACEK techniques with ACET effect into consideration, as ACET effect exists in a much wider range of frequency.

1.3.3 AC Electrothermal effect:

AC electrothermal effect is a phenomenon, which is caused by the interaction between the applied electric field and the temperature gradients. These temperature gradients are generated by conductivity (σ) and permittivity (ε) gradients induced by heating effects. The relationship between the applied voltage (V_{rms}) and the pumping velocity (u) is $u \propto V_{\text{rms}}^4$.

Fluid flow:

The type of fluid flow in a channel is generally determined by Reynolds number. The Reynolds number (Re) is the ratio of inertial forces to the viscous forces for a flowing liquid.

$$Re = \frac{\rho u L}{\mu} = \frac{u L}{\nu} \quad (\text{Eq 11})$$

Where ρ denotes the density of the fluid, u is the velocity of the fluid with respect to the object, L is a characteristic length, μ is the dynamic viscosity of the fluid, and ν is the kinematic viscosity of the fluid. In general, If the Reynolds number is <2000 then the flow is considered to

be a laminar flow. As Re is proportional to L , it is much less than 2000 in the microfluidics where dimensions are usually in microscale or nanoscale. In Laminar flow regime, the viscous forces are dominant and are characterized by smooth, constant fluid motion.

Governing equations:

Navier-stokes equations can be used to determine the fluid flow velocity in the microchannel. Once the velocity is determined other factors such as temperature and pressure can be found using different equations. As explained in the definition of ACET non-uniform electric field causes temperature gradients. The temperature gradient obtained from the energy balance equation is

$$k\nabla^2 T + \frac{1}{2} \sigma E^2 = 0 \quad (\text{Eq 12})$$

Where E is the magnitude of the electric field, σ is the electrical conductivity and k is the thermal conductivity of the fluid. For a homogeneous medium E can be calculated from Laplace's equation $\nabla^2 V = 0$ with $E = -\nabla V$.

Since the temperature distribution affects the temperature gradients the permittivity and conductivity of the fluids are as below:

$$\nabla \varepsilon = \left(\frac{\partial \varepsilon}{\partial T} \right) \nabla T \quad (\text{Eq 13})$$

$$\nabla \sigma = \left(\frac{\partial \sigma}{\partial T} \right) \nabla T \quad (\text{Eq 14})$$

These will induce a free charge density ρ_q in the bulk of the fluid: which is given by the equation:

$$\rho_q = \nabla \cdot (\varepsilon E) = \nabla \varepsilon \cdot E_0 + \varepsilon \nabla \cdot E_1 \quad (\text{Eq 15})$$

Now, the electrical body force becomes

$$f_e = (\nabla \varepsilon \cdot E_0 + \varepsilon \nabla \cdot E_1) E_0 - \frac{1}{2} E_0^2 \nabla \varepsilon \quad (\text{Eq 16})$$

According to the charge conservation equation

$$\frac{\partial \rho_q}{\partial t} + \nabla \cdot (\rho_q u) + \nabla \cdot (\sigma E) = 0 \quad (\text{Eq 17})$$

Where, $\rho_q u$ is the convection current and σE is the conduction current. The divergence of the perturbation field $\nabla \cdot E_1$ is given by

$$\nabla \cdot E_1 = \frac{-(\nabla \sigma + i\omega \nabla \varepsilon) \cdot E_0}{\sigma + i\omega \varepsilon} \quad (\text{Eq 18})$$

Hence, Eq 9 can be rewritten in a time average scale as:

$$f_e = \frac{1}{2} \text{Re}[(\nabla \varepsilon \cdot E_0 + \varepsilon \nabla \cdot E_1) E_0^* - \frac{1}{2} |E_0|^2 \nabla \varepsilon] \quad (\text{Eq 19})$$

Substituting equation Eq 11 and equation Eq 12 gives the body force in terms of the applied field

$$f_e = \frac{1}{2} \text{Re} \left\{ \left[\frac{(\sigma \nabla \varepsilon - \varepsilon \nabla \sigma) \cdot E_0}{\sigma + i\omega \varepsilon} \right] E_0^* - \frac{1}{2} |E_0|^2 \nabla \varepsilon \right\} \quad (\text{Eq 20})$$

Combing Eq 6, 7, and 13, time averaged electrical force density can be obtained as follows

$$f_e = \frac{1}{2} \text{Re} \left\{ \frac{\sigma \varepsilon (\alpha - \beta)}{\sigma + i\omega \varepsilon} (\nabla T \cdot E_0) E_0^* - \frac{1}{2} \alpha \varepsilon |E_0|^2 \nabla T \right\} \quad (\text{Eq 21})$$

For an aqueous solution in the temperature of 293K , the permittivity and conductivity can be assumed as linear functions of temperature.

$$\left(\frac{1}{\varepsilon} \right) \left(\frac{\partial \varepsilon}{\partial T} \right) = \alpha = -0.4\% K^{-1} \quad (\text{Eq 22})$$

$$\left(\frac{1}{\sigma} \right) \left(\frac{\partial \sigma}{\partial T} \right) = \beta = 2.0\% K^{-1} \quad (\text{Eq 23})$$

The Eq 14 induces flow motion and the velocity of the micro flows can be determined by the Navier-Stokes and mass conservation equations:

$$-\nabla p + \eta \nabla^2 \mathbf{u} + \mathbf{f}_e = 0, \nabla \cdot \mathbf{u} = 0 \quad (\text{Eq 24})$$

Where \mathbf{u} is the velocity field vector, η is the dynamic viscosity and p is the pressure. From the equations mentioned above it is evident that magnitude of the ACET force depends on the applied electric field strength and the temperature gradients.

1.4 Micropumps

To make the fluids flow through the microchannels two kinds of pumps can be used i.e. mechanical pumps and non-mechanical pumps.

Mechanical Pumps: Mechanical micropumps use the motion of a solid (such as a gear or diaphragm) or a fluid to generate the pressure difference needed to move fluid. The most common mechanical displacement micropumps are diaphragm pumps. Their actuation mechanisms are varied. They need a physical actuator for the pumping and they have moving parts. The actuator should run itself with dead volume (V_o) in the chamber. Fluid flow is achieved by oscillatory or rotational pressure forces. The oscillations create pressure (ΔP), which is a function of the stroke volume (ΔV) inside the chamber and produced by the actuator. The compression ratio is defined as $\epsilon = \Delta V / V_o$ [1], examples of mechanical micropumps include piezoelectric, electrostatic, thermo pneumatic, electromagnetic, bimetallic, Ion Conductive Polymer Films (ICPF) and Shape Memory Alloy (SMA) [2]. These micro scale displacement pumps often have a pump chamber, actuator and valves. Susceptibility to bubbles can be significantly problematic to these pumps and/or their valving. To avoid these complexities non-mechanical pumps are often used in LOC applications.

Non-Mechanical Pumps: Non-mechanical pump has to transform specific non-mechanical energy (electroosmotic, electrohydrodynamic, magneto-hydrodynamic, electrowetting, etc.) into kinetic momentum to drive fluid sample into the microchannels. Non-mechanical pumps can be

further categorized as being electrical, chemical, or magnetic. Electro and magneto-kinetic micropumps convert electrical and magnetic energy into fluid motion. The pumping is continuous, so the resulting flow is generally constant/steady. Electrokinetic micropumps often use an electric field to pull ions within the pumping channel, in turn dragging along the bulk fluid by momentum transfer due to viscosity. Magneto kinetic micropumps typically use Lorentz force on the bulk fluid to drive microchannel flow. Dynamic pumps do not usually have valves; they obtain directionality from the direction of the applied force [3] other nonmechanical pumps include Electro-Osmotic micropumps [4], and DC Electro-Osmotic (DCEO) Micropumps [5].

Two main challenges to EO micropumps are: microchannel-blocking bubbles and low stall pressure (typical of EO micropumps with an open channel). The large currents generated in the open channel may produce bubbles; electrolysis and reactions at the electrodes produce ions that can contaminate the sample and generate the bubbles. High pressure can be built up by using very small channels or by keeping the channel densely packed. Some of the disadvantages of EO micropumps often are alleviated by controlling the packing of particles in the channel [6].

AC Electro-osmotic (ACEO) Micropumps: ACEO flow is a viable micro-scale pumping mechanism for conductive or electrolytic solutions. Unlike the deprotonation on the channel surface in DCEO flow, electrodes positioned on the channel boundary provide the charge necessary to establish an electric double layer. Asymmetric electrodes induce an electric field and draw the diffused layer charges along the electrode surface. The advantage of ACEO pumps includes possible achievement of high velocities for very small voltages less than 10V. Also, as voltages increase within the range, flow can be reversed, making this pump type bi-directional. Reverse-flow velocities have been found to be larger than forward flow velocities [7].

1.5 Micromixers

Micromixer elements, micromixers, and microstructured mixers typically have flows in the sub-ml/h, ml/h–l/h and 10–10,000 l/h ranges, respectively, thus covering the whole flow range up to the conventional static mixers and being amenable to analysis and chemical production as well. When used at the upper flow limit, microstructured mixers can act as process-intensification (PI) equipment.

Micromixing Principles: Due to the absence of turbulence in microfluidic devices, mixing depends solely on molecular interdiffusion. The diffusive flux, e.g. of a solute, equals $D \cdot A \cdot \nabla c$, i.e., diffusion coefficient times the interfacial surface area times the gradient of species concentration. Accordingly, diffusive mixing can be optimized by maximization of the constituting factors. Leaving an enhancement of the diffusion coefficient, e.g. by an appropriate temperature rise, aside one is left with the maximization of $A \cdot \nabla c$. So, the art of micromixing translates to an efficient maximization of interfacial surface area and concentration gradient. Above all convective diffusion enhancement is commonly employed in mixing devices.

Reynolds number ($Re = U \cdot d/\nu$), the Peclet number, $Pe=U d/D$, and the Fourier number, $Fo =Tr/Tm$, are commonly used as dimensionless groups to characterize convective/diffusive problems. Here U , d , ν denote the average velocity, the hydraulic diameter or the transverse diffusion distance which are assumed to be of the same order of magnitude, and the kinematic viscosity. Tr , Tm denote the average residence time and the diffusive mixing time, defined as $Tr =L/U$ and $Tm =d^2/D$, where L denotes the longitudinal length. For laminar uniaxial flows, the mixing length Lm is found to be proportional to Pe times the channel width.

Mixing Efficiency Determination:

The most common and simplest way to judge on mixing in micromixer structures is done by flow visualisation via dilution-type experiments usually by the aid of microscopic-, photo-, video- or high-speed camera. This is done by contacting dyed and transparent liquid streams (passive mixing) or standing volumes (active mixing) in a type of photometric experiment. In fluorescence experiments, visualisation is achieved by fluorescent streams; in a commonly applied reaction variant, mixing is proven by quenching of fluorescent streams. We determined mixing efficiency using dye and a camera.

CHAPTER II

LITERATURE REVIEW

2.1 ACEO & ACET Micropumping

Micropumping using ACEO has been one of the intensive research fields over the past few years for microfluidic applications, and ACEO micropumps have shown great potential for lab-on-a-chip applications with its low-voltage and low-frequency operation, and capability for flow control. However, ACEO tends to produce recirculating flows as reported in the literature. To produce net flow, it is necessary to break ac electric field symmetry. So far, this objective has been achieved by various asymmetric electrode geometries. The examples include asymmetric interdigitated electrodes [1–3], orthogonal electrodes [4], and three-dimensional ACEO pump [5].

One of the strategical approach is to induce asymmetry polarization of the electrodes in a pair of electrodes by applying biased ac signals, to generate unidirectional flow of fluids [6]. When a voltage is applied over the electrodes in electrolytes, electrode surfaces will become populated with net charges and the process is known as polarization. The two types of electrode polarizations generate opposite surface charges for EO surface flows. By applying asymmetric electric signals to the electrodes, the two electrodes in a pair will exhibit different polarizations and strength of the double layer at the electrode/electrolyte interface. As a result, a unidirectional Maxwell force will be exerted on the fluid, leading to throughflow pumping.

A common configuration of ACEO electrodes is the “side-by-side” planar electrode pairs, as shown in Figure 1. For the electrode configuration shown here, the electric fields at the electrode surface have both tangential and normal components.

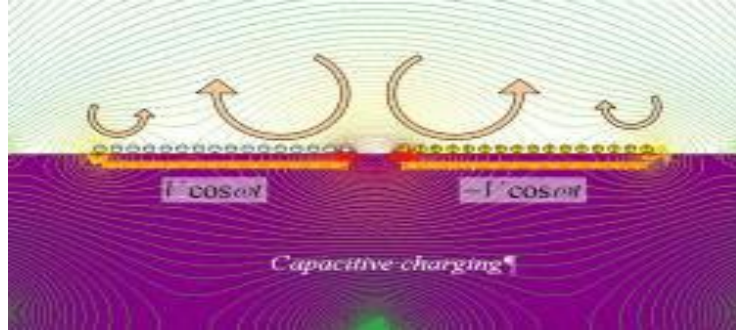


Figure 1: Electric field distribution showing four counter-rotating vortices above a pair of coplanar electrode.

The normal E-fields induce charges/ions in the nanometer thick double layer, and the tangential E-fields drive the ions along the electrode surfaces. Because charges in the double layer change signs with electric fields, the flow directions are maintained over ac cycles.

ACEO induced by a pair of symmetric electrodes exhibits mirror symmetry, so that counter-rotating local vortices are produced above the electrodes. There are two major vortices close to the inner edges of the electrodes and two minor vortices at the outer edges. The minor vortices are caused by fringing fields and are noticeably weaker than the major vortices. This phenomenon was experimentally demonstrated in [8-9]. To use ACEO for pumping, it is essential to break the symmetry of electric fields within an electrode pair, so that the major vortex on one electrode will overcome the resistance from the other to produce a unidirectional flow. This can be achieved by spatial asymmetry in electrode design as people typically do, or by polarization asymmetry as presented in this paper.

With asymmetric geometries, the flow direction is predetermined by electrode design. When an electric potential is applied to the electrodes that are exposed to electrolyte, the electrode surface becomes polarized with charges. The electrodes can attract counterions from the electrolyte known as capacitive or induced charging, or can generate ions from electrochemical reactions at the electrodes known as Faradaic charging. With ac fields, electrode polarization by capacitive charging has been widely recognized as the mechanism responsible for ACEO. We demonstrated the net transport of fluid based on asymmetric electrode polarization using the Orthogonal electrode pattern.

When a fluid bulk is subjected to an electric field a viscous drag force is developed due to the rise in the temperature gradient. This flow is termed as ACET flow [11]. One of the earliest research on ACET flow was carried out by applying a non-stationary drive fluids in which an array of electrode attained a peak velocity of $\sim 180 \mu\text{m s}^{-1}$ at $35V_{pp}$, 100 kHz with fluid conductivity 9.3 mS m^{-1} , which was higher than the conventional electrohydrodynamic (EHD) micro pumps. This demonstration showed practical possibilities of non-uniform electric signals producing high fluid velocity, which is useful for micropumping applications. In most of the biological applications the assay needs to be moved from the centralized lab to the point of care, to perform immunoassay diagnostics. To achieve this, process of testing must be faster, as well as more portable, while maintaining the performance characteristics. Tending towards these needs many formats of miniaturized immunoassays have been developed in the recent years. Some of them include various forms of LOC devices which can perform fluid processing and detection steps on a single chip. On chip sample preparation reduces sample preparation time and shorter test times. Despite of having smaller length scales, these assays can be limited in response to the diffusion time of the analyte to a stationary legend. Addressing the need for faster

assay binding Hong, *et al* [12] demonstrated the application of ACET effect to induce vortices in a pressure driven flow through system improving the binding rate in the electrolyte. This is one of the earliest, to achieve transport of fluid in diffusion-limited reaction increasing the binding rate factor by seven when compared to conventional binding process.

Recently, ACET effect was used to induce vortices with a pressure driven flow-through system ($\sigma = \sim 0.6 \text{ S m}^{-1}$), improving binding rate of antigen-antibody [13]. Wu, *et al* [13] demonstrated pumping with applied voltage levels less than $15 \text{ V}_{\text{rms}}$ for fluid conductivity of $0.02\text{-}1 \text{ S m}^{-1}$ with fluid velocity reaching up to $1000 \mu\text{m s}^{-1}$. While working with high conductivity fluids, excessive temperature rise happens and buoyancy force will dominate over ACET effect. For aqueous solutions, the ratio of ACET to buoyancy force can be approximately given as $\frac{f_E}{f} = 7.95 \times 10^{-12} \cdot \left(\frac{\nabla T}{\Delta T}\right) \cdot E_{\text{rms}}^2$ so, to induce ACET effect high $\frac{\nabla T}{\Delta T}$ is required.

Choosing the electrodes with good conductivity ensures high $\frac{\nabla T}{\Delta T}$ thus, inducing the required ACET flow. Wu, *et al* [13] used a pair of electrodes as shown in the Figure 2a.

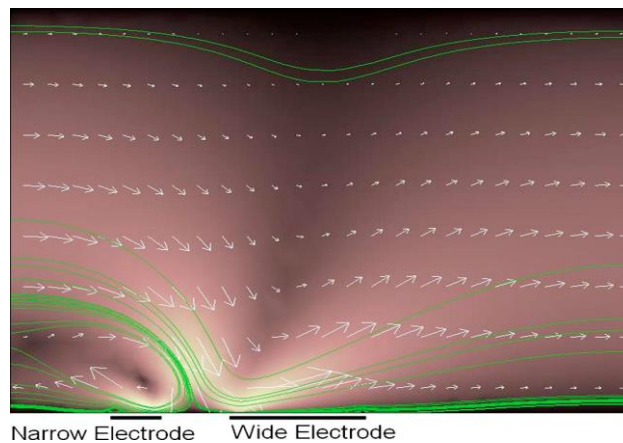


Figure 2a: Simulation of net flow produced by ACET over two electrodes of different widths. [13]

The electrodes present in the bottom of the channel act as a heat source, producing stronger electric fields than the in the bulk fluid. With the electrodes acting as a source of heat, at room temperature maximum temperature gradient ∇T was found to be occurring in the proximity of the electrodes. Along with the temperature gradient, the induced charge density and electric field strength were also highest close to the electrodes. As a result, the ACET force near over the electrodes drags the fluid defining the flow field. In this type of arrangement, the more flow occurs over the wider electrode, so a net flow with a direction is generated above the wider electrode. With this kind arrangement, a flow rate of $\sim 150 \text{ nl s}^{-1}$ was achieved by applying 7 V_{rms} at 200 kHz on a bulk fluid with conductivity $\sigma = 0.224 \text{ S m}^{-1}$. After demonstrating the possibilities of asymmetrical electrodes in the micropumping Wu, *et al* [13] went further to investigate pumping and proposed a pin-line “T” configuration, which had higher degree of asymmetry. The “T” configuration setup was shown in the Figure 2b.

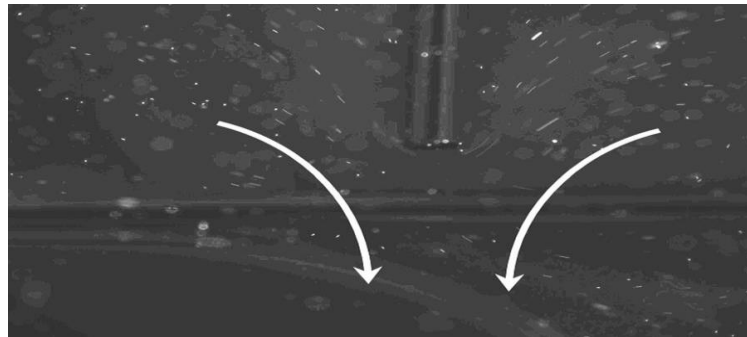


Figure 2b: Pumping by T electrode at $14 \text{ V}_{\text{rms}}$, 1 MHz . [13]

The fluid was observed moving from back of the pin towards the tip and across the transversal electrode. The flow rates of over 1 mm/s were observed at the pin tip, when the fluid with conductivity $\sigma = 0.21 \text{ S m}^{-1}$ was actuated at $14 \text{ V}_{\text{rms}}$. This was ten times higher when compared to the arrangement shown in Figure 2a. The fluid field was found be dominating by

the flows over the transversal electrode were the thermal gradients were high. This design achieved unidirectional flow through geometric asymmetry. One part this thesis optimized the “T” shaped configuration to study the flow pattern at various voltage and frequency levels.

Hong, *et al* [11] demonstrated a numerical study on the ACET flow in the same configuration as a planar electrode. This research also demonstrated that the highest temperature gradients appear at the region where the field strength is also strongest. They achieved unidirectional flow by using electrodes having different lengths. They determined that the smaller electrode length can achieve greater fluid velocities. Explanation of two internal forces, Coulomb force and dielectric force was given as follows. Coulomb force depends on applied AC frequency and electrolyte’s electrical charging time. This electrical charging time is given by $\tau = \epsilon / \sigma$ where σ and ϵ are the conductivity and electrical permittivity respectively. The Coulomb force decreases with the increase of frequency, but is almost independent of frequency when $\tau \ll 1/2\pi f$, and becomes negligible when $\tau \gg 1/2\pi f$ [11]. The dielectric force, however, is frequency-independent. Therefore, there exists a crossover frequency f_c , where the two electrical forces are equal in magnitude and cancel each other. f_c can be given by the equation $f_c = \frac{\sigma}{2\pi\epsilon} \left| 1 - 2\frac{\beta}{\alpha} \right|^{\frac{1}{2}}$ where ϵ and σ are the permittivity and conductivity of the medium respectively, $\alpha = -0.4\%K^{-1}$ and $\beta = 2.0\%K^{-1}$. f_c can also be calculated from $f_c \approx \frac{\sqrt{11}}{2\pi\tau}$ [14]. When the applied frequency reaches cross over frequency (f_c), the net velocity becomes almost zero. This shows that electrothermal flow velocity is large when Coulomb force is dominating dielectric force. Therefore, to achieve a high electrothermal flow velocity, the electrical charging time τ needs to be much smaller than $1/2\pi f$, where the electrothermal flow is only due to the Coulomb force and frequency independent.

The direction and magnitude of the fluid may not be unidirectional throughout the experimental process. To address this issue [15] proposed a DC biased ACEK flow in which the magnitude and the flow direction can be governed by varying the DC and AC voltages applied. Yang, *et al* [15] carried out a convincing research to prove that DC biased ACEK can be used in efficient mixing, trapping and pumping applications.

As mentioned, Fluid velocity increases with the fluid conductivity as energy dissipation increases [13] making Joule heating proportional to the fluid conductivity and therefore dependent on fluid used and also variations in the fluid arising from chemical reactions. The use of external heating element into the Electrothermal flow provides independent control of the temperature gradients established in the system. A resistive heater [16] is incorporated in between the interdigitated electrodes to provide bulk electrothermal pumping. Yua, *et al* [17] applied 4 V_{rms} at 100 kHz on a similar electrode arrangement and introduced an external heat flux which increased the fluid flow velocity to $\sim 112\mu\text{m s}^{-1}$ from $\sim 10\mu\text{m s}^{-1}$ when there was no external thermal source. Also, in case of asymmetric electrode pair a single dominant force was observed when an external illumination was applied as a heat source to of the electrodes in the electrode pair. This kind of asymmetrical illumination creates a transverse thermal gradient across the electrodes. Interaction of electric field with the conductivity gradients creates a single dominant vortex creating a unidirectional flow. Other research works to focus on external heat source include Discretized electrodes [18]; a middle electrode is centered between two asymmetrical electrodes to achieve forward and backward pumping action.

2.2 Micromixing

AC EK has been used in various biochemical and biomedical applications for mixing of bioparticles such as live cells, bacteria, proteins and DNA. By taking the advantage of the ACEK

forces, this thesis applied AC EK techniques to investigate the possibility of micromixing in a circular electrode pattern. This section deals with the previous studies involved in micromixing. Even though DEP is negligible while dealing with biomedical samples having conductivity $> 0.1 \text{ S m}^{-1}$ some of the earlier research works studied micromixing using DEP. Deval and Lee *et al* [19-20] demonstrated chaotic DEP micromixing in a simple microchannel integrated with microelectrodes at the bottom of the surface. They explained the production of chaotic advection with the variation of channel geometrical properties and applied electric field. Saddle point regions were generated due to the interaction between applied electric field and fluid velocity with respect to time and space. Chaotic vortices were generated due to the exponential stretching rate as the particles undergo a series of stretching and folding at these saddle points. This makes the diffusion mixing faster leading to an efficient mixing rate [21]. Gunda, *et al* [22] used a similar electrode arrangement but, with triangular electrodes at the bottom of the microchannel surface and presented a numerical study attaining 97% mixing efficiency for four pair of electrodes used in the experiments.

Later, Sigurdson, *et al* [23] used the ACET effects to develop an immunosensor to study binding of antigen in the sample to antibody present on the microchannel. They suggested that ACET can be more advantageous than ACEO in generating fluid motion in electrolyte buffers having high conductivity and the binding rate can be enhanced by choosing appropriate Peclet number and Damköhler number [23]. Through this model binding rate was increased by a factor of 7, for 6 V_{rms} applied electric potential demonstrating electrothermally-generated stirring in the microchannel can increase binding rates in the suspended medium. Closely following this work Feldman, *et al* [24] investigated binding enhancement using electrothermal stirring with a biotin-streptavidin assay. They immobilized biotin on the bottom of a microwell and suspended

streptavidin in a high conductivity buffer. Experimental and numerical simulation of this work demonstrated that ET microstirring can be used to increase the binding up to a factor of 9 for 10 V_{rms} applied voltage. They also calculated the precision level to 7% by repeating the process for 51 times. This provides an insight on microstirring efficiency to improve binding rates. Feng, *et al* [25] came up with experimental and numerical solutions on ET flows. They made use of ACET for mixing fluids and then cleansing the microcavities from the contaminants trapped inside. By creating chaotic flow using ACET techniques they were able to increase the mixing efficiency by three orders of magnitude when compared to normal diffusion based mixing.

Recently, A pair of coplanar electrodes with a sinusoidal interelectrode gap were studied in a Y shaped microchannel under high fluid conductivity ($\sigma = 0.5 \text{ S m}^{-1}$) inducing ACET flow [26]. This model attained mixing index greater than 90% by applying 30 Vp-p voltage at 5 MHz frequency. Gunda, *et al* [27] demonstrated analytical and numerical solutions of ACET forces along the channel length and height, pointing out that the variation in those will vary the kind of ACEK forces acting in fluid channel using different electrode arrangements.

Application of voltage levels ranging from 0-8 V_{rms} at 100 kHz frequency an array of circular microelectrode pairs [28] fabricated on the perimeter of a fluidic channel as shown in the Figure 3 also achieved acceptable fluid flow velocities.

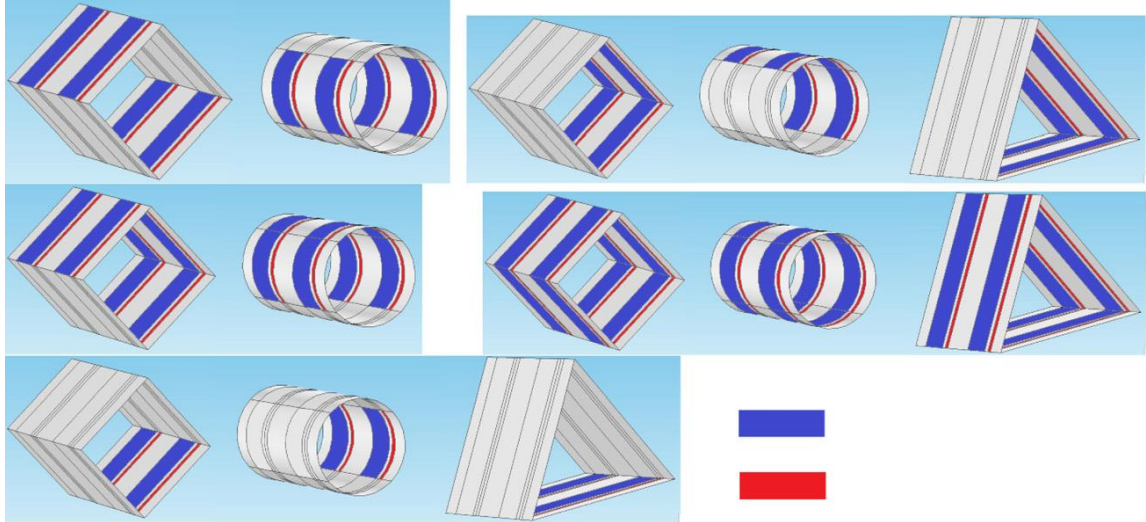


Figure 3: Different actuation configurations of side electrode arrays. (a) Two opposing arrays (Side1), (b) two sidelong arrays (Side2), (c) three arrays (Side3), (d) all side arrays (Side4), and (e) conventional single array (Side5). The fluidic channel has a hydraulic diameter of 300 μm and the substrate thickness is 200 μm . [20]

The results showed that the ACET flow rate can be increased by increasing the number of electrode arrays used in the micropump. Although the fabrication of micropumps with three (Side3) and four (Side4) electrode arrays can be more challenging, devices with two arrays (Side1) can be easily fabricated using the same technology as for conventional single array (Side5) devices. The number of side electrode configurations and their corresponding patterns has been shown to be effective in increasing the ACET flow. Additionally, it was shown that acute angles in fluidic channel geometries, such as triangular cross sections, can give rise to highly localized temperature gradients, and consequently higher electrothermal force. However, the temperature increase can be challenging, but it appeared to be safe for biofluid applications ($<40^{\circ}\text{C}$) if relatively low actuation voltage $V_{\text{rms}} < 5$ are used. Also, governing the heat generation to avoid any unrelated interference can be addressed by optimizing the electrode geometries

[21] a novel circular electrode arrangement was used in this thesis to study ACET flows in a circular device.

2.3 Particle Manipulation

Particle manipulation and separation techniques have been of interest to many research groups worldwide for various biomedical applications, including cell concentration, separation, patterning trapping and positioning [29]. These methods have facilitated the development of cost-effective point-of-care (POC) devices that can rapidly collect, prepare and analyze human biological samples. Diverse diagnostic approaches have been exploited to manipulate particles using lab-on-a-chip (LOC) platforms; however, dielectrophoresis (DEP), as the sample preparation stage of a POC device, presents unique features; including the differentiation between particles is based merely on the particles' dielectric properties (electrical conductivity and permittivity) determined by the phenotype of the respective particles, and the high selectivity and efficacy of particles manipulation on micro and nano levels [30].

DEP is a non-invasive method that describes the movement of polarizable particles when subjected to a non-uniform electric field. The basis for generating the DEP force is the interaction between the particle's dipole and the spatial gradient of the electric field [31]. DEP has been extensively employed as a potential technique to manipulate viruses [32], proteins [33], bacteria [34], DNA [35], spores [36], algae [37], parasites [38] and nano-sized latex particles [39]. In addition, DEP has been used in research on cell lysis [40] and to determine the characteristics of wide range of the yeast cells [41] and the mammalian cells, such as neurons [42], leukemia cells [43], platelets [44], sperm cells [45], and cancer cells [46].

CHAPTER III

DEVICE FABRICATION

Most of the microfluidic devices share a similar fluidic platform. The fabrication, design, and operation of the fluidic systems in these devices are based on those developed for microfluidics used in different applications. This chapter describes the basic ideas involved in designing and fabrication process of microfluidic devices. Materials most commonly used in fabricating microfluidic systems and the techniques developed for fabricating them were summarized the following section. Which is then followed by the description of the characteristics of flow in these systems.

3.1 Properties of PDMS

Polydimethylsiloxane (PDMS) has been one of the most widely used material in the research and development of microfluidics. PDMS is an optically transparent elastomer whose stiffness can be controlled by varying the mixing ratio of the base and the curing agent. The fabrication of microchannels in PDMS is simple and straightforward. The use of PDMS as a material allows prototyping of devices, to demonstrate the fabrication process and testing of new concepts. The physical and chemical properties of PDMS also make possible the fabrication of devices with a useful range of functions, ranging from particle trapping to frequency-tunable micropumping.

Most research in microfluidic systems is being carried out using PDMS and other polymers. Fabrication process using polymers is simple, more flexible, inexpensive, and less

time taking than in silicon or glass. For example, one can come across problems such as the formation of sharp fragments by using hard materials, these can be avoided using PDMS and other polymers. Because of PDMS having several attractive properties which make it suitable as a material for prototyping of microfluidic devices capable of supporting a wide range of applications, both the devices in this thesis took the advantage of using PDMS in their fabrication process. In this thesis, Dow Corning Sylgard 184 Silicone Elastomer PDMS (Figure 4) has been used to fabricate the proposed devices.

3.1.1 Mechanical Properties of PDMS:

PDMS is tunable because of its Young's modulus, which is typically around 750 kPa [47]. Due to its elastomeric nature, it can deform easily, confined to surfaces, and can easily attain the features of a mold including internal features without damaging the mold or itself. Microfluidic channels or shapes on the micro or even micron scale can therefore be reproduced with high constancy in PDMS by molding. Some of the properties of the PDMS were given in the **Table 1**. Examples of the PDMS-based microstructure include MCP (microcontact printing), μ FN (microfluidic network), CE (capillary electrophoresis [48-50]), multilayered structures with valving capability [51], Using composite stamps composed of two layers a stiff layer supported by a flexible layer of PDMS, replication of features below 1 nm [52-53]. Changing the periodicity of the grooves on the grating or the lens, and the respective diffraction pattern generated or the focal properties of the lens [54-55].



Figure 4: Sylgard 184 silicone elastomer base and curing agent

Property	Value
Mass density	0.97 kg/m ³
Young's modulus	360-870 KPa
Poisson ratio	0.5
Tensile or fracture strength	2.24 MPa
Residual stress on silicon	
Specific heat	1.46 kJ/kg K
Thermal conductivity	0.15 W/m K
Dielectric constant	2.3-2.8
Electrical conductivity	4x10 ¹³ Ωm
Magnetic permeability	0.6x10 ⁶ cm ³ /g
Biocompatibility	Nonirritating to skin, no adverse effect on rabbits and mice, only mild inflammatory reaction when implanted
Hydrophobicity	Highly hydrophobic, contact angle 90-120°
Melting Point	-49.9–40°

Table 1: Properties of PDMS (Source: MIT Material Property Database) [56]

Solvent Compatibility of PDMS: PDMS is nontoxic to proteins and cells. It is slowly permeable to water but, it is completely permeable to oxygen (O₂) and carbon dioxide (CO₂). It is, therefore, suitable for biological applications: for example, live cells can be directly cultured on it [57].

PDMS compatibility with water, and most polar organic solvents (such as methanol and glycerol); however, it might show signs of swelling, in nonpolar organic solvents (such as pentane and chloroform) [58], as it absorbs nonpolar solutes from aqueous solutions. To reduce the absorption of solutes and the swelling nature by nonpolar organic solvents, one can coat the surface with a glass-like layer using sol-gel chemistry [59], or modify PDMS with silica particles [60].

3.2 Fabrication process of orthogonal electrode

A microscopic glass slide was spin coated (Figure 5) with PDMS using a mixture of Sylgard 184 base and curing agents at 10:1 ratio respectively. PDMS helps in making the glass slide hydrophobic which in turn helps in increasing the pumping velocity. An orthogonal electrode arrangement was made by using, two Signatone (SE-10T) electrodes which were placed to represent T shape. The sharp edge electrode placed vertically creates better electrical potentials thus eliminating the need for higher voltages. The spacing between the two electrodes is 140µm and the width of each electrode is 250µm as shown in the Figure 6. These two electrodes are covered with Coverwell perfusion chamber (Grace Bio-Labs PC8R-0.5) with 8x9mm Diameter and 0.6mm Depth sealed using epoxy glue.



Figure 5: Laurell WS-650-15B Spin Coater



Figure 6: Orthogonal electrode pair on a PDMS coated glass slide

3.3 Fabrication process of circular electrode pattern

A conducting strip (copper) was placed on a microscopic glass slide to actuate the copper electrode. This copper electrode is basically an uninsulated conductive wire, which was carefully amputated at 1.2 mm length having 0.5 mm diameter or thickness. Copper electrode was then electrically soldered onto the conducting strip under a microscope to achieve maximum conduction between the copper strip and the electrode. After this, a rectangular box having the length of the glass slide was placed with copper electrode in its center. This box was then filled with Polydimethylsiloxane (PDMS: mixture of Sylgard 184 base and curing agents at 10:1 ratio respectively) covering 0.6 mm of the copper electrode from the base. Necessary precautions were taken to ensure that the surface of the PDMS was flat and even. PDMS was then cured at

room temperature for 48 hours, curing time can be reduced by using microwave oven but, it was not used in this case because of the soldering parts.

After the curing process, rectangular box was carefully removed leaving a fine rectangular piece of PDMS slab. On this PDMS slab a Coverwell perfusion chamber (Grace Bio-Labs PC8R-0.5) with 8x9mm diameter and 0.6mm depth was kept with the copper electrode in its center as shown in the Figure 7. Then, a circular ring made up of a steel alloy with platinum coating of 3.6 mm diameter was placed and sealed to prevent fluid from leaking. This circular ring was actuated by a conducting nickel wire.

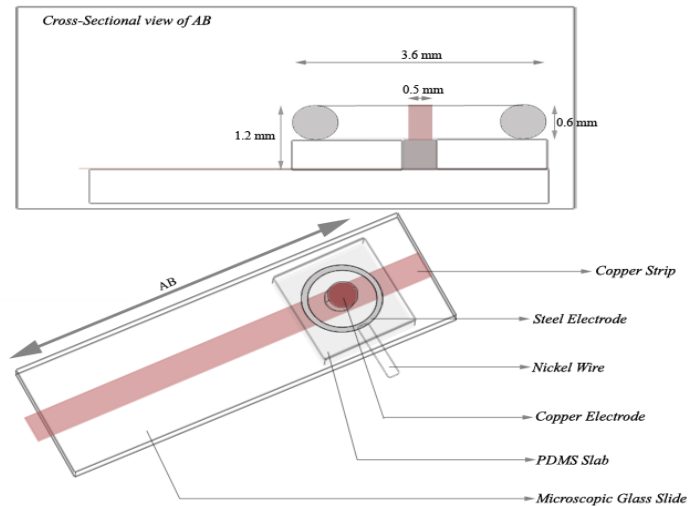


Figure 7: Circular electrode pair device with cross-sectional view

CHAPTER IV

ANALYSIS AND SIMULATION

4.1 COMSOL for microfluidics

COMSOL Multiphysics is a powerful interactive environment for modeling and solving all kinds of scientific and engineering problems. The software provides a powerful integrated desktop environment with a Model Builder where you get full overview of the model and access to all functionality. With COMSOL Multiphysics you can easily extend conventional models for one type of physics into Multiphysics models that solve coupled physics phenomena—and do so simultaneously. Accessing this power does not require an in-depth knowledge of mathematics or numerical analysis. Using the built-in physics interfaces and the advanced support for material properties, it is possible to build models by defining the relevant physical quantities—such as material properties, loads, constraints, sources, and fluxes—rather than by defining the underlying equations. You can always apply these variables, expressions, or numbers directly to solid and fluid domains, boundaries, edges, and points independently of the computational mesh. COMSOL Multiphysics then internally compiles a set of equations representing the entire model. You access the power of COMSOL Multiphysics as a standalone product through a flexible graphical user interface (GUI) or by script programming in Java or the MATLAB® language (requires the COMSOL LiveLink for MATLAB).

Heat Transfer Module: The Heat Transfer Module supports all fundamental mechanisms of heat transfer, including conductive, convective, and radiative heat transfer (both surface-to-surface and surface-to-ambient radiation). Using the physics interfaces in this module along with inherent Multiphysics capabilities of COMSOL Multiphysics you can model a temperature field in parallel with other physics.

The Heat Transfer Module Model Library contains models, with Multiphysics couplings, that cover applications in electronics and power systems, process industries, and manufacturing industries

Microfluidics Module: The Microfluidics Module is a collection of tailored physics interfaces for the simulation of microfluidic devices. It has a range of tools to address the specific challenges of modeling micro- and nanoscale flows. Physics interfaces that address laminar flow, multiphase flow, flow in porous media, and rarefied flow such as free molecular flow, slip flow, and transitional flow are available. Enhanced capabilities to treat chemical reactions between dilute species are also included. In addition to the standard tools for modeling fluid flow, interfaces between fluids can be modeled by the Level Set, Phase Field, and Moving Mesh physics interfaces, making it possible to model surface tension and multiphase flow at the microscale [61].

4.2 Micro PIV system

Micro PIV system in our lab consists of the following parts (Figure 8):

- A) YAG70-15-QTL Laser power unit
- B) YAG70-15-QTL Liquid light guide assembly
- C) Laser pulse synchronizer
- D) CCD camera

- E) Nikon Eclipse LV150N Microscope
- F) Insight 4G Data Acquisition, Analysis and Display package
- G) Tecplot Focus Software
- H) Function generator and
- I) High-Voltage Amplifier

This laser is provided with an offset time (Δ) which emits laser when the camera is about to capture an image. The glass slide was placed under the microscope and the two Electrodes were energized by a 15 MHz function generator connected with a high voltage amplifier. Emission of the laser and the image capturing device will work synchronously tracing the fluorescent particle movement in the micro chamber.

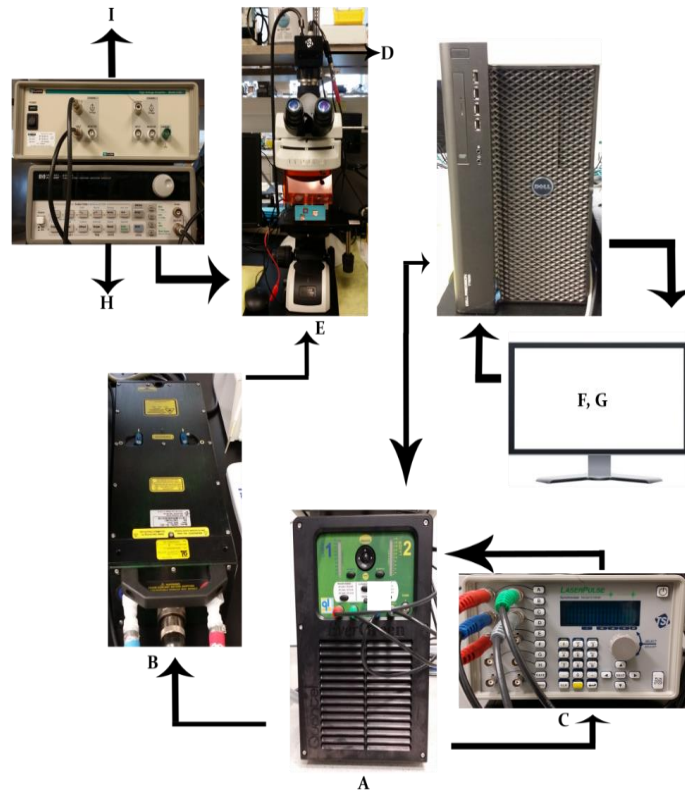


Figure 8: Micro PIV System

Using Insight 4G as the user interface we carried each of the experimental run by capturing and analyzing 100 Frames for every run. These 100 frames were processed after checking spatial calibration and masking the boundaries. Insight 4G processing generates an excel sheet which consists of vector positions of the particles. This software detects the particle flow and creates vector files, which are then used to plot the graph by Tecplot Focus 2013R1 software add-on available in the Insight 4G. Insight 4G can overlap more than 100 frames (depends on the available RAM space) to create vector data which makes the results accurate.

4.3 Experimental Procedure for orthogonal electrodes

Experiment were performed using three fluids. 1) De-ionized (DI) water having $18.32\mu\text{S}/\text{cm}$ conductivity and Fluorescence particles with $1\mu\text{m}$ in diameter. cm 2) Tap water with $1532\mu\text{S}/\text{cm}$ and 3) Phosphate Buffered Saline (PBS) solution with $15\text{mS}/\text{cm}$ having 10:1 concentration of DI water and PBS (10X) which is then mixed with 540nm fluorescence particles with $1\mu\text{m}$ in diameter.

4.4 Numerical Analysis of circular electrode pair

Circular electrode pattern was simulated using FEMLAB – COMSOL Multiphysics software (version 5.2a). Two-dimensional geometrical model used for the simulation is shown in the Figure 9a. A circular electrode pair was placed on a glass slab which consists a circular ring (Metal: Steel) with 3.6 mm diameter and a copper electrode with 0.5 mm diameter. The empty domain between the steel electrode (circular ring) and the copper electrode was filled with water.

Numerical steps involve several steps, first step uses Laplace's equation to determine the electric field distribution. A cross-sectional view of the resultant electric field strength is shown in the Figure 9b.

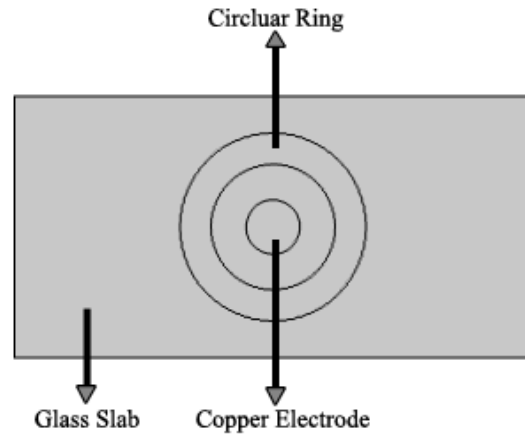


Figure 9a: Simulated geometrical model in FEMLAB-COMSOL Multiphysics

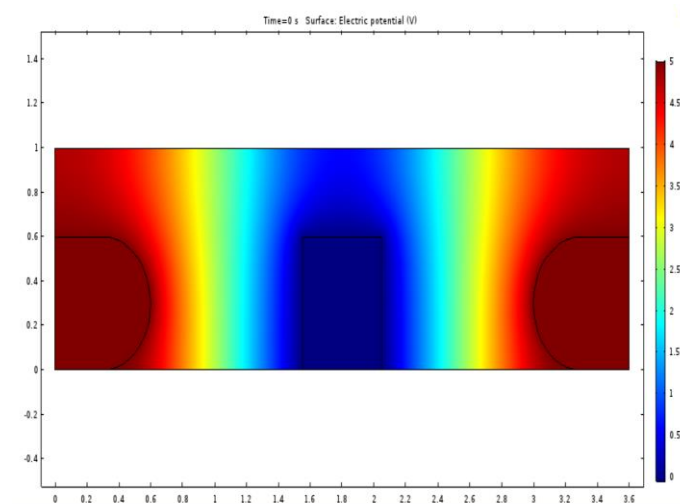


Figure 9b: A cross-sectional view of COMSOL simulated electrical potential distribution in the Circular electrode pair.

During the next step, energy equation (f_e) yields temperature field distribution using the electric field. Finally, thermal gradients and electric gradients were put into the Navier-Stokes equation to obtain the fluid velocity in the domain or chamber, which consists the experimental fluid. Electric field simulation was done using electric current module. Steel electrode was set at certain electric potential and other boundaries were kept at neutral and insulated. The entire

experimental setup was kept at ambient temperature and the electrodes were assumed to be isothermal. Then using the laminar flow module and frequency dependent study, the applied AC frequency was varied to obtain simulated results at required voltage levels and frequencies. The electric field strength at 5V indicates that the electric field was maximum over the steel electrode and becomes insignificant over the copper electrode. It is evident that the tangential components of the electric field over the steel electrode induce microflows.

The result of the simulation for 5V at 800kHz for fluidic conductivity $\sigma = 1.62 S/m$ is shown in the Figure 10. At this point, the direction of the fluid was unclear from the simulations carried out, we focus on the flow pattern in between the electrodes. The direction of the fluid was demonstrated in the experimental section.

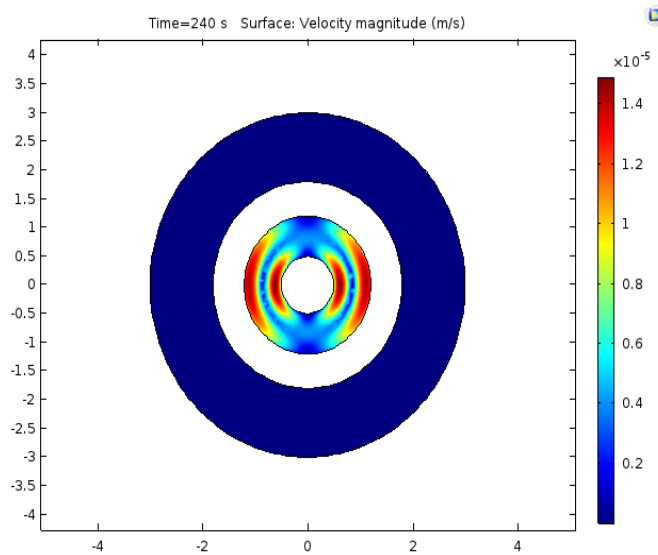


Figure 10: COMSOL simulation results for fluid conductivity $\sigma = 1.62 S/m$ at 5V, 800kHz.

CHAPTER V

RESULTS AND DISCUSSION

5.1 Orthogonal Electrode Pattern

Experiments with Deionized water are conducted at 500Hz to 1.2MHz frequency range with the voltage varied from 6Vpp to 20Vpp. The electric density is strong at the tip of the sharp electrode and the net flow is observed to be high at the tip of the sharp electrode where zeta potential is high. At low frequency and low voltage, the fluid flows along the vertical electrode towards the lower electrical density (away from the gap between the electrodes). At higher frequencies, the chances of forming a double layer is very low due to the decrease of zeta potential [62], thus decreasing the velocity and the colloidal stability at the surface of the electrode.

As, AC electroosmosis shows no effect at higher frequencies this makes AC electrothermal effect responsible for the fluid flow at high frequency and high voltage range where the thermal gradients of the fluid cause a net flow in the fluid bulk. The maximum velocity graph for 20Vpp at a frequency range of 500Hz to 1.2MHz was shown in Figure 11.

The fluid flow due to the AC electro osmosis which is away from the sharp tip and the fluid flow due to the AC electro thermal effect which is towards the tip and the gap cancel each other. The frequency at this point is called transition frequency and the flow appears to be steady without any vortices. The velocity of the flow depends on the applied electric signals as well as the conductivity of the fluid experiments conducted on the fluid with conductivity 1532 μ S/cm

stands as a good example for the behavior of conductive fluid due to the AC electrothermal effect.

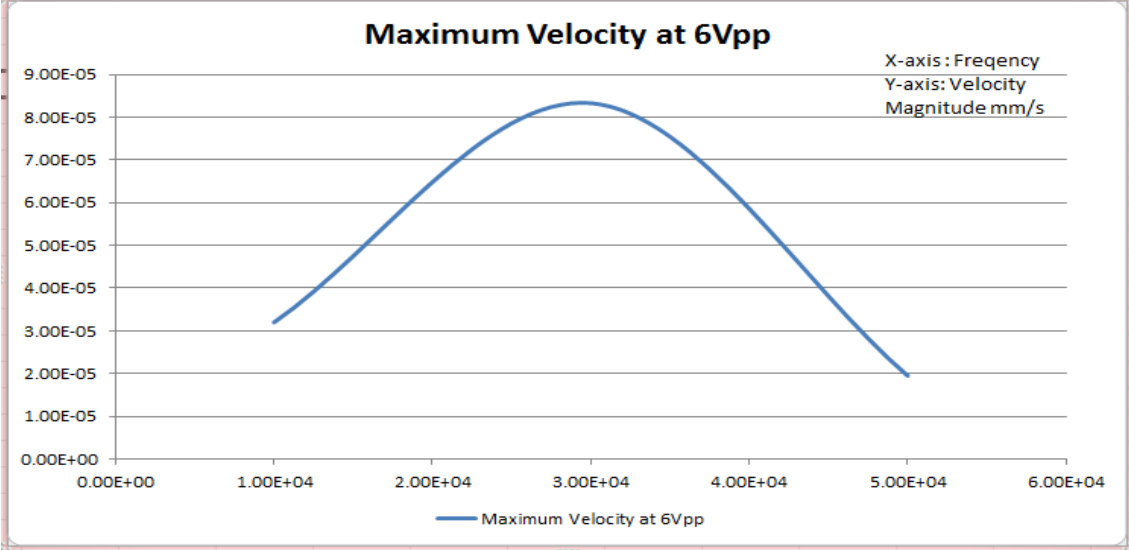


Figure 11a: Maximum velocity plot at 6Vpp representing a bell shape from 10 kHz to 50 kHz

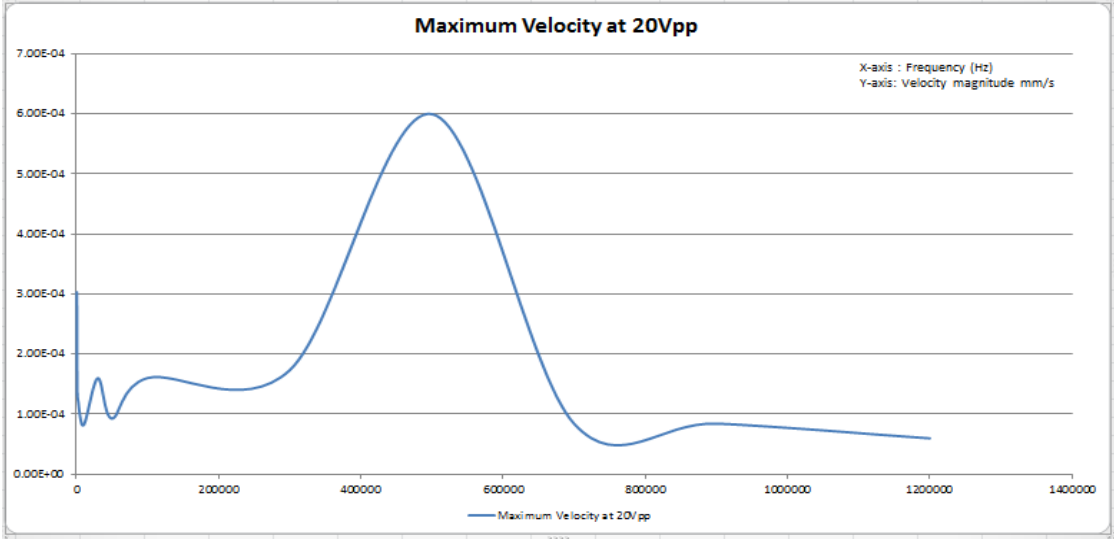


Figure 11b: Experimental results representing the maximum velocity at 20Vpp at a frequency range of 500Hz to 1.2MHz.

5.1.1 Micro-pumping: The mechanism behind ACET effect depends on Joule heating. Joule heating occurs when an external electric field is applied across the electrodes immersed in a fluid. The non-uniform electric field across the electrode generates temperature gradient near to the electrodes. The interaction between the temperature gradient and the applied electric field induces permittivity and conductivity gradients in the fluid causing bulk fluid motion. In our experiments pumping action was demonstrated at different frequencies for each chosen fluid.

From the experimental results pumping was observed both in ACEO and ACET frequency levels as shown in the Figure 11a and Figure 11b. However, pumping due to ACEO effect was insignificant when compared to the ACET as the experimental results showed that ACEO effect was insignificant after 100 KHz and most of the peak velocities were found at the frequency greater than 100 KHz. Maximum velocities were recorded while ACET effect was in effect. This was consistent with the previous research work. From the Table 2 it is evident that increasing the conductivity influences the pumping frequency in an increasing fashion, however after crossing the crossover frequency the velocity decreases with the increase in the frequency.

Fluid	Conductivity	Frequency at which pumping was observed
DI water	18.32 μ S/cm	3 KHz – 1 MHz
Tap water	1532 μ S/cm	5 KHz – 1 MHz
PBS	15mS/cm	80 KHz – 1 MHz

Table 2: Observed frequency range for the pumping of the three fluids with different conductivities at 15Vpp.

The horizontal electrode acts as a source of heat with stronger electric fields, because electric fields are stronger on the surface of the electrode than in the bulk fluid. ACET force near

the electrode determines the flow field [6], as the electrodes are asymmetric the fluid in contact with the electrodes experiences similar thermal gradients, making the flow to act along the wider (horizontal) electrode Figure 12. So, a net flow is generated along the axis of the wider electrode.

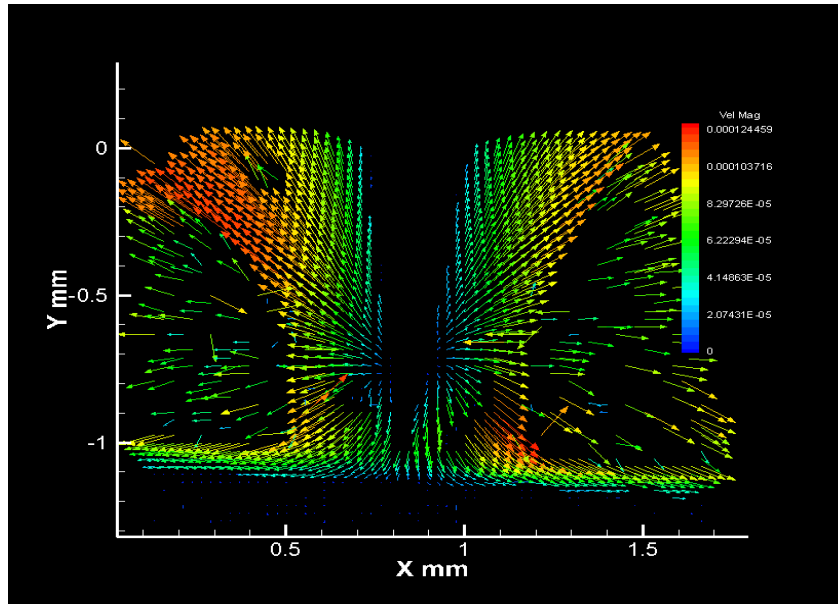


Figure 12: The figure shows the pumping action of the fluid (PBS) at 80Khz and 15Vpp obtained from Tecplot Focus software

5.1.2 Micro-mixing: Experimental results showed when the mixing is performed in a conventional Y shaped structures [63], the mixing process may require longer micro channels. This can be avoided by the application of ACET and ACEO [8]. During the steady state in AC EO all the electrical field lines will be tangential to the surface of the conductor as the EDL is fully charged. Two non-linear AC electroosmotic slip velocities are formed with the interaction of the induced double layer and the external field. These slip velocities give rise to two symmetric vortices which help in mixing of two different fluids. Again, we must remember that increasing the frequency reduces the thickness of the double layer which creates a steady flow

due to ACET effect. In our experiments, we observed the formation of vortices using tap water from 5 KHz to 800 KHz at 15Vpp. The strongest vortices with maximum velocity around them were observed at 5 KHz and 100KHz Fig .5. These experimental results may prove that the mixing through non-planar orthogonal electrodes can be possible by both ACEO and ACET effects. With our non-planar electrode structure micromixing can be done by introducing a secondary fluid to the chamber in which primary fluid is present. If the secondary fluid is introduced on the primary fluid through the inlets of the coverwell perfusion chamber, the fluids can be mixed by two symmetrical vortices shown in (Figure 13).

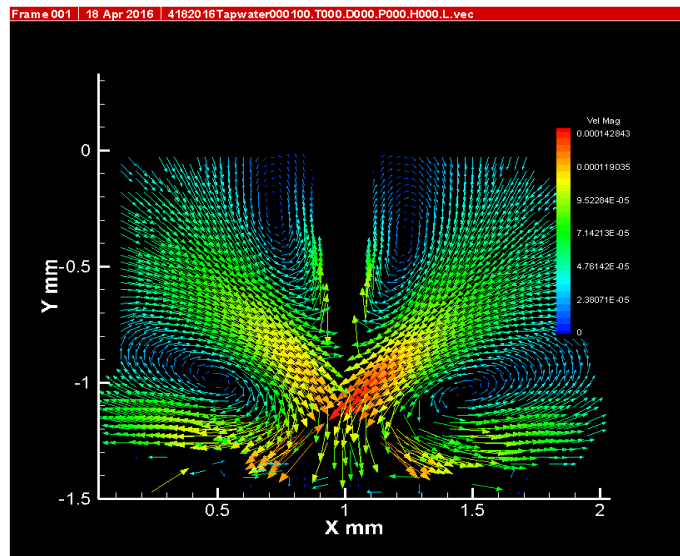


Figure 13: Experimental results show the formation of vortices at 100KHz 15Vpp obtained from micro-PIV Tecplot

5.1.3 Bio/nano-particle Trapping: After transferring the particles to the detection sites or stagnation sites by ACEO and ACET effects, DEP force can be used as a trapping force to capture the particles as a holding mechanism. The velocity at the tip of the electrode is high where the field gradient is maximized [64]. So, when the particles having the size greater than

1 μ m (Escherichia coli K-12 nutrient agar can be used to grow harmless bacteria to the size of 5 μ m) approached the converging point the DEP force attracts the particles to the tip of electrodes. Since the DEP range is short, this would be effective only near to surface of the electrode. If the cross over frequency of the cells is known DEP can be used to concentrate and separate the particles as the particles experience positive and negative DEP forces.

The present orthogonal electrode pair was constructed on a PDMS which makes the surface hydrophobic (Contact angle 105°). Increase in the surface characteristics by introducing Nano-composite fiber makes the surface super-hydrophobic (contact angle 150°) which may yield better results over the current experiments.

5.1.4 Comparison with previous work:

Recalling the work of Wu, *et al*, the flow rates exceeded 1 mm/s at 14 V_{rms} for $\sigma = 0.21 S/m$, which is suitable for pumping applications. For better comparison let us consider the results obtained using tap water with conductivity $\sigma = 0.15 S/m$. The highest peak to peak voltage used in this thesis on orthogonal electrode device for tap water was 15V_{pp} which is equal to $\sim 5V_{rms}$. At 15 V_{pp}, 500 kHz the observed velocity was 390 μ m/s. Neglecting electrolysis and other potential barriers at 15 V_{rms} the proposed Orthogonal electrode pattern in this thesis can achieve velocities greater than 1mm/s. Therefore, it is evident that the implementing sharp edged electrode in the existing orthogonal electrode pattern can increase pumping velocity. This thesis also proposes that the orthogonal electrode pattern can be used as a multi-functional system as shown in the previous sections.

5.2 Circular Electrode Pattern

Experiments with two conductive buffered solutions were conducted at 500Hz - 5 MHz frequency range with the voltage range varied from 1V_{pp} to 7V_{pp}. Generation of bubbles and

electrolysis were observed over the voltage level of 7Vpp this can be explainable as the electrical and thermal conductivity of steel are much smaller than the copper, due to these limitations experiments were conducted up to 7Vpp which was found be maximum safe voltage applicable to the steel electrode used in the experiments.

At low frequency and low voltages (<4Vpp) the induced fluid flows can negligible when compared to the fluid velocities at higher voltage levels (5Vpp-7Vpp). At 50 kHz and < 4Vpp fluid velocity due to ACEO dominated the flow velocity due to ACET effect. However, at higher voltage(>4Vpp) and higher frequency (>100kHz) maximum peak velocity was found while the fluid velocity is due to the ACET effect. **Figure 14a and 14b**, demonstrates the fluid velocities obtained at 50kHz, 500kHz and 1MHz with the voltage levels varying from 1Vpp to 7Vpp with fluid conductivities 1.632 S/m and 0.073 S/m respectively. The obtained velocities were higher in the case of fluid with conductivity 1.632 S/m over 0.073 S/m. Thus, indicating that the increase in fluid conductivity increases the fluid velocity under the same conditions.

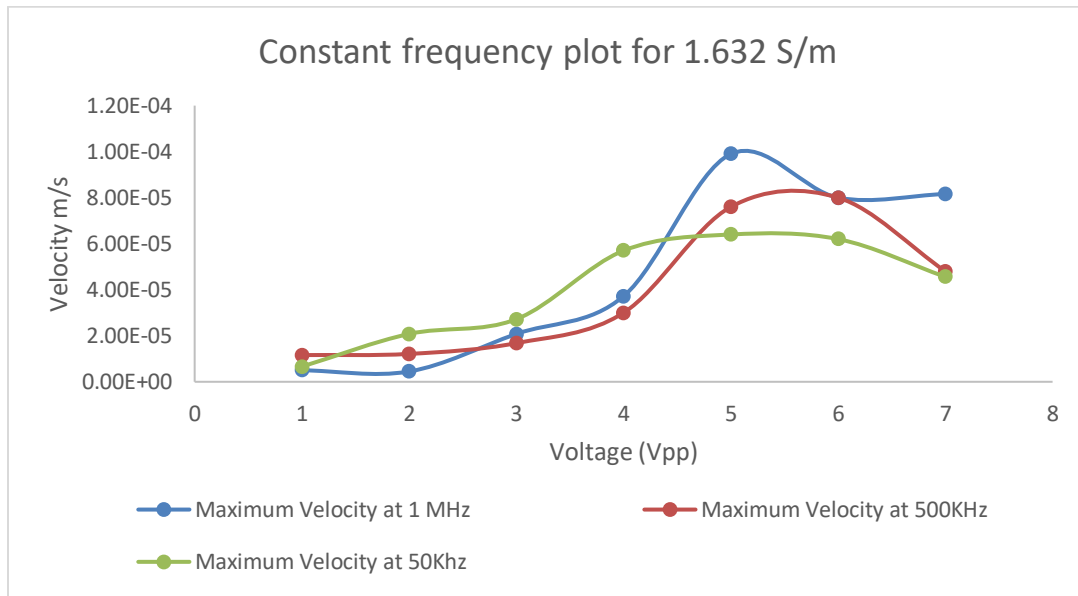


Figure 14a: Graphical representation of fluid velocities at 50kHz, 500kHz and 1MHz with applied voltage varying from 1Vpp to 7Vpp. $\sigma = 1.632$ S/m

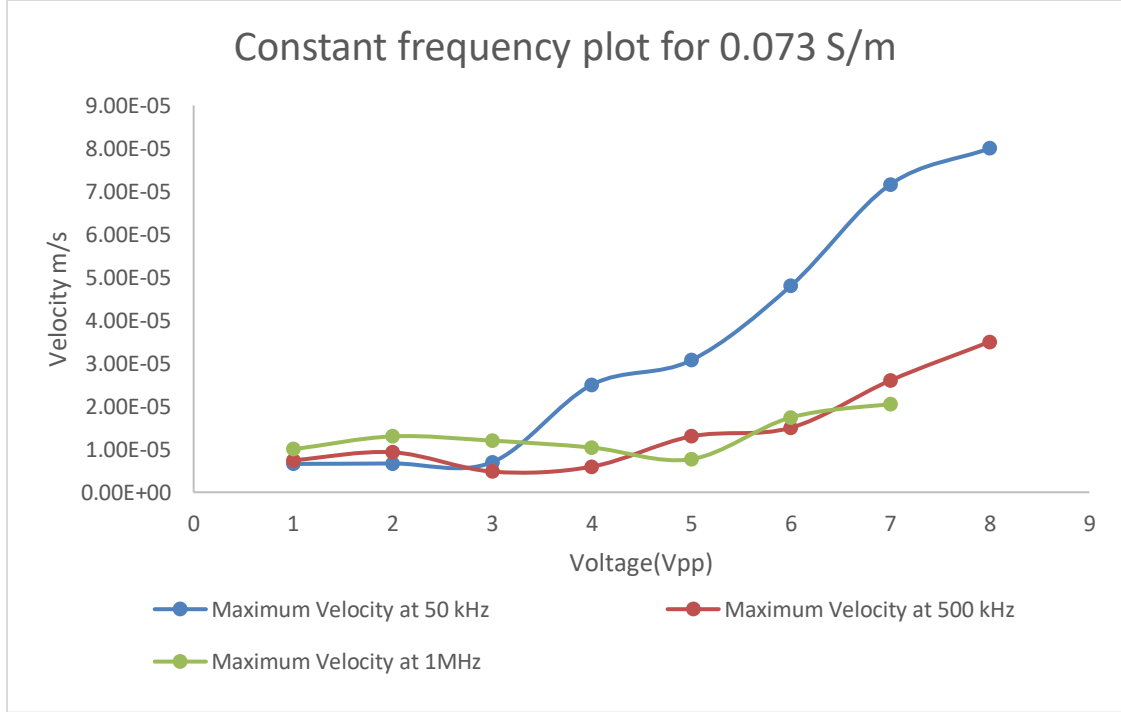


Figure 14b: Graphical representation of fluid velocities at 50kHz, 500kHz and 1MHz with applied voltage varying from 1Vpp to 7Vpp. $\sigma = 0.073$ S/m.

Coulomb force depends on applied AC frequency and electrolyte's electrical charging time. This electrical charging time is given by $\tau = \epsilon / \sigma$ where σ and ϵ are the conductivity and electrical permittivity of the medium respectively. The Coulomb force decreases with the increase of frequency, but is almost independent of frequency when $\tau \ll 1/2\pi f$, and becomes negligible when $\tau \gg 1/2\pi f$. The dielectric force, however, is frequency-independent. Therefore, there exists a crossover frequency f_c , where the two electrical forces are equal in magnitude and cancel each other. f_c can be given by the equation $f_c = \frac{\sigma}{2\pi\epsilon} \left| 1 - 2\frac{\beta}{\alpha} \right|^{\frac{1}{2}}$ where ϵ and σ are the permittivity and conductivity of the medium respectively, $\alpha = -0.4\%K^{-1}$ and $\beta = 2.0\%K^{-1}$ at 293^0 K. f_c can also be calculated from $f_c \approx \frac{\sqrt{11}}{2\pi\tau}$. When the applied frequency reaches cross over frequency (f_c), the net velocity becomes almost zero. This shows that electrothermal flow velocity is large when Coulomb force is dominating dielectric force. Therefore, to achieve a high electrothermal flow

velocity, the electrical charging time τ needs to be much smaller than $1/2\pi f$, where the electrothermal flow is only due to the Coulomb force and frequency independent. Assuming, that the permittivity of the medium is equal to the permittivity of the water ($710 * 10^{-12} C^2 N^{-1} m^{-2}$) values of τ and cross over frequency (f_c) were shown in Table 3. This gives a clear picture that the higher conductivity fluids can be electrically charged in lesser periods of time, which in turn increases the cross over frequency.

Fluid Conductivity	Fluid's electrical charging time (τ)	Cross over frequency (f_c)
0.073 S/m	9.86×10^{-12}	5.3×10^7 Hz
1.62 S/m	4.3504×10^{-10}	1.2×10^9 Hz

Table 3: values of τ and f_c for fluid conductivities 0.073 S/m & 1.62 S/m.

In our experiments, decrease in velocity for 1.62 S/m conductivity fluid was observed at ~4MHz figure 15a and for 0.073 S/m it was observed at ~1MHz figure 15b. In figure 15a the fluid velocity was observed to be depreciating over 4 MHz attributing to the dominance of dielectric force, this trend continues in figure 15b but the velocity became negligible at ~1MHz because the fluid conductivity in figure 15b is less than the fluid conductivity in figure 15a. The numerical cross over frequencies derived earlier were higher than the observed frequencies, which can be explained by certain factors such as the electrical properties of the medium and the electrodes may change over certain period due to the repeated process of the experiments and also the change in the fluid properties due to the presence of the fluorescence particles and the colored dye which is introduced later to determine the micromixing efficiency.

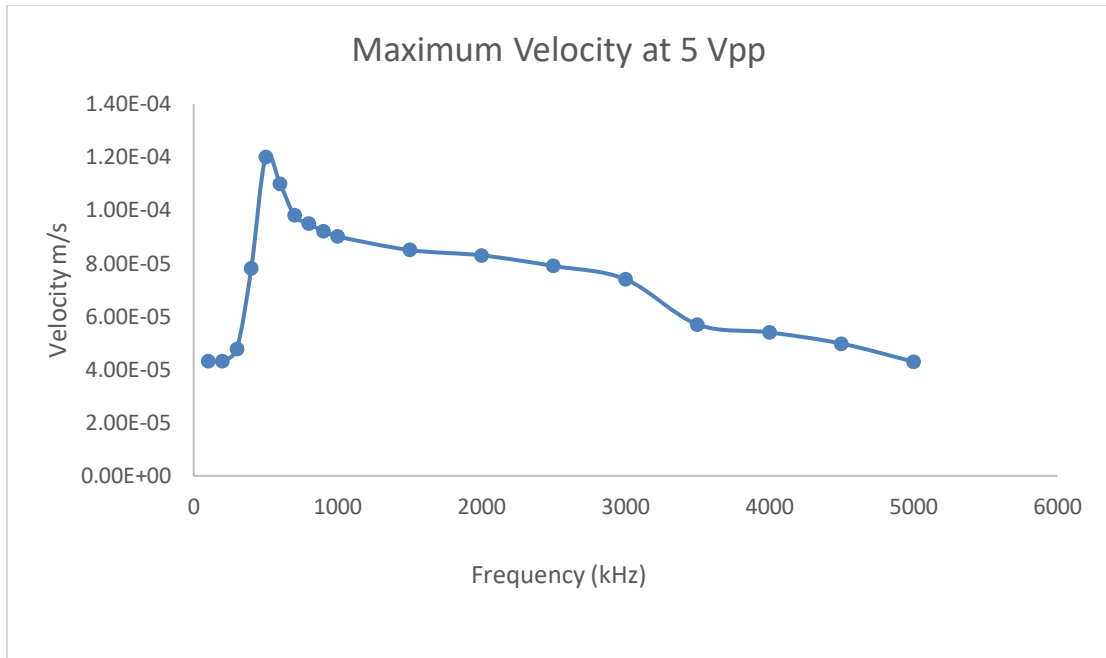


Figure 15a: Peak velocity of the fluid (conductivity = 1.632S/m) at 5Vpp with frequency ranging from 100kHz to 1MHz.

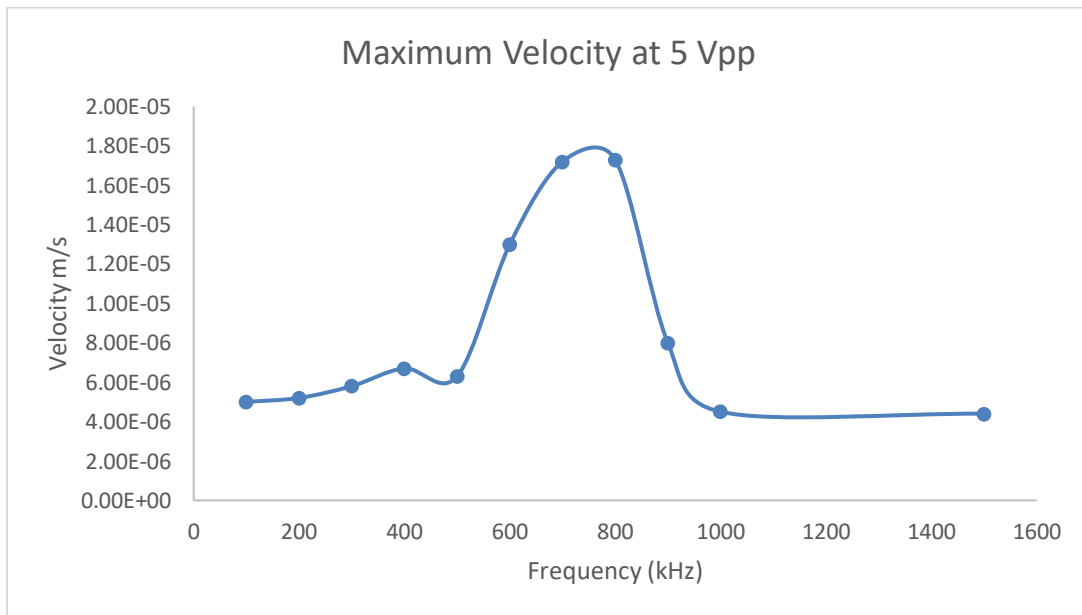


Figure 15b: Peak velocity of the fluid (conductivity = 0.073S/m) at 5Vpp with frequency ranging from 100kHz to 1.5 MHz.

5.2.1 Comparison between the experimental and simulated results

Laminar flow module in COMSOL simulation software was used to determine the velocity of the fluid therefore, the simulated results were more oriented on the velocity attained in the circular chamber and the magnitude of the flow but, during the experiments we observed chaotic flow as shown in the figure 16.

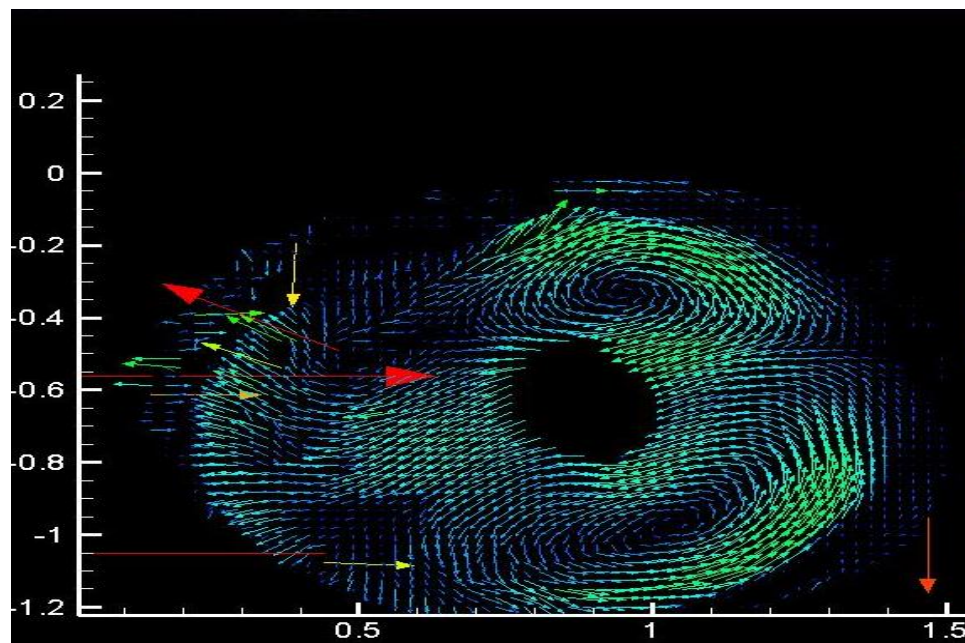


Figure 16: Generation of chaotic flow at 5Vpp, 600kHz with fluid conductivity 1.632 S/m.

Fluid velocities obtained from the simulation and the experiments were shown in the figures 17a, 17b, 17c ($\sigma = 1.62 \text{ S/m}$) and 18a, 18b, 18c ($\sigma = 0.073 \text{ S/m}$). The velocity pattern observed from the experiments and the simulation shows similar patterns but, disparity was observed by a scale of 1 order in magnitude.

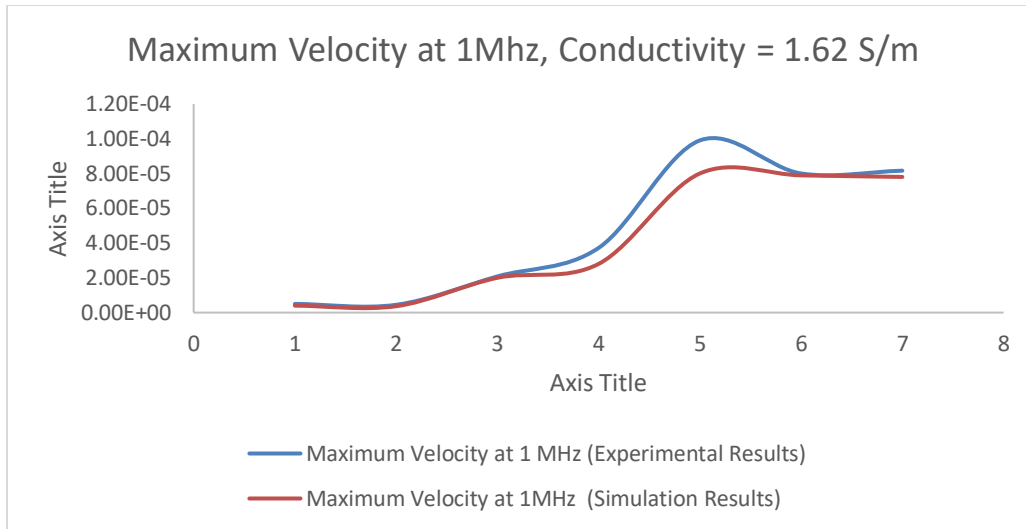


Figure 17a: Disparity between the experimental and simulated results obtained on the fluid with conductivity 1.62 S/m at 1 MHz and different voltage levels.

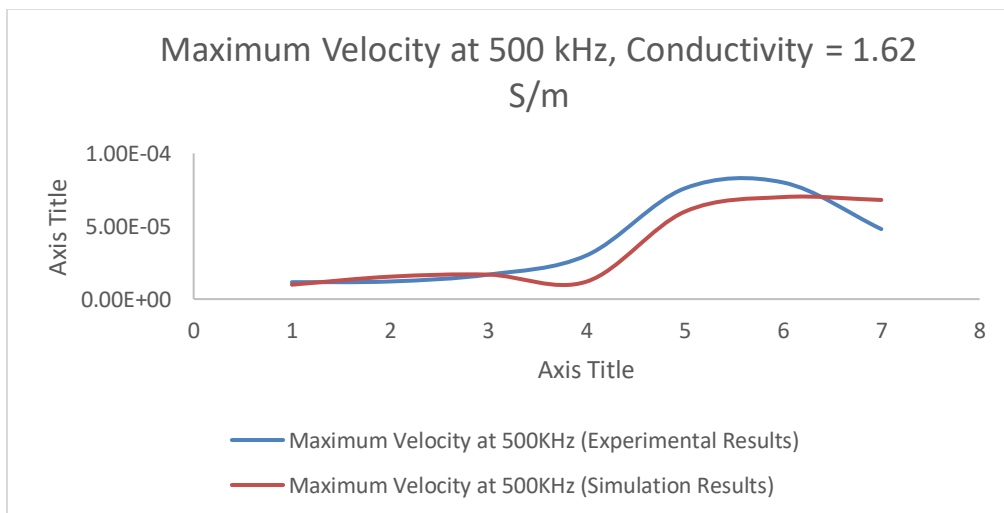


Figure 17b: Disparity between the experimental and simulated results obtained on the fluid with conductivity 1.62 S/m at 500 kHz and different voltage levels.

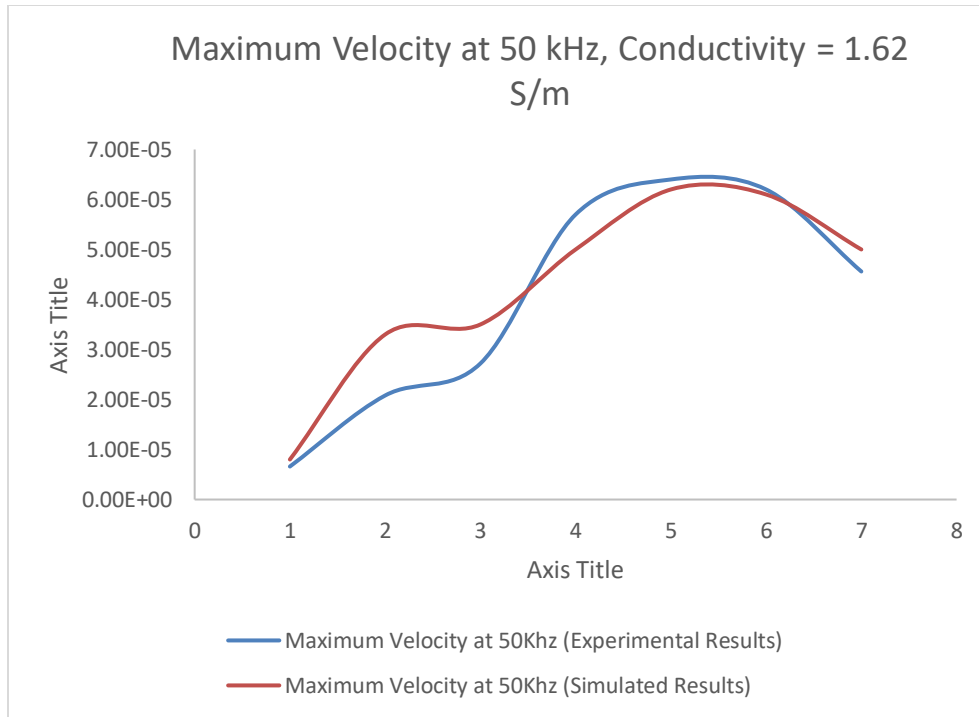


Figure 17c: Disparity between the experimental and simulated results obtained on the fluid with conductivity 1.62 S/m at 50 kHz and different voltage levels.

For fluid with conductivity 0.073 S/m decrease in velocity was observed at frequencies below 1 MHz (Fig 18b and 18c). Experimental device used in this thesis does not have an inlet and outlet valve which is must in the module used by the simulation software. The suspension of the fluid was done by colloidal suspension. However, unavailability of these features might not be the sole reason for the observed discrepancy. Ongoing investigation is being carried out to better explain this difference.

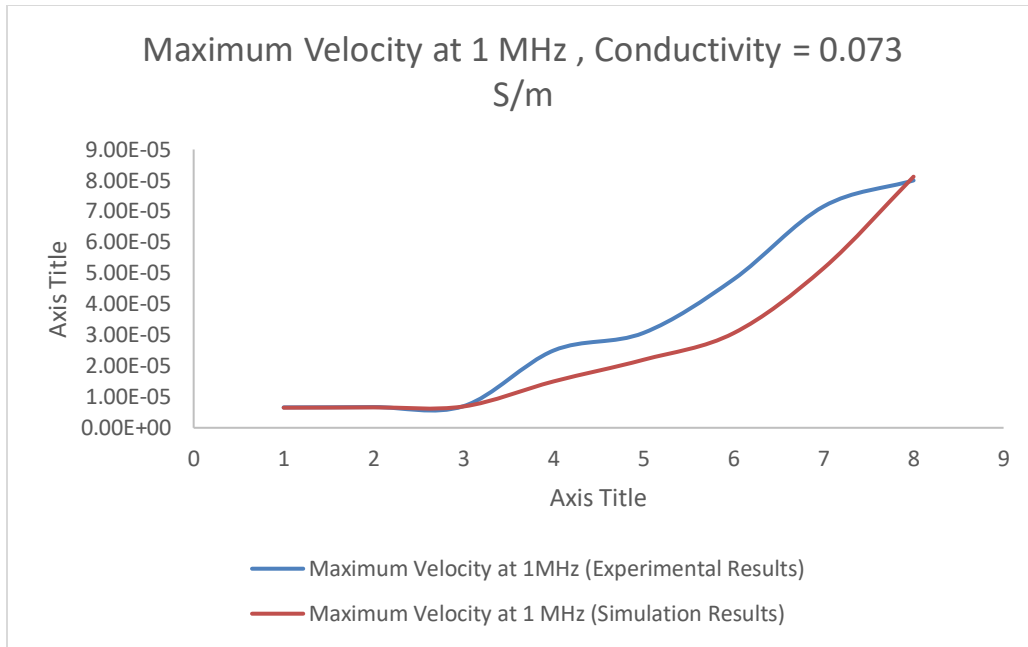


Figure 18a: Disparity between the experimental and simulated results obtained on the fluid with conductivity 0.073 S/m at 1 MHz and different voltage levels.

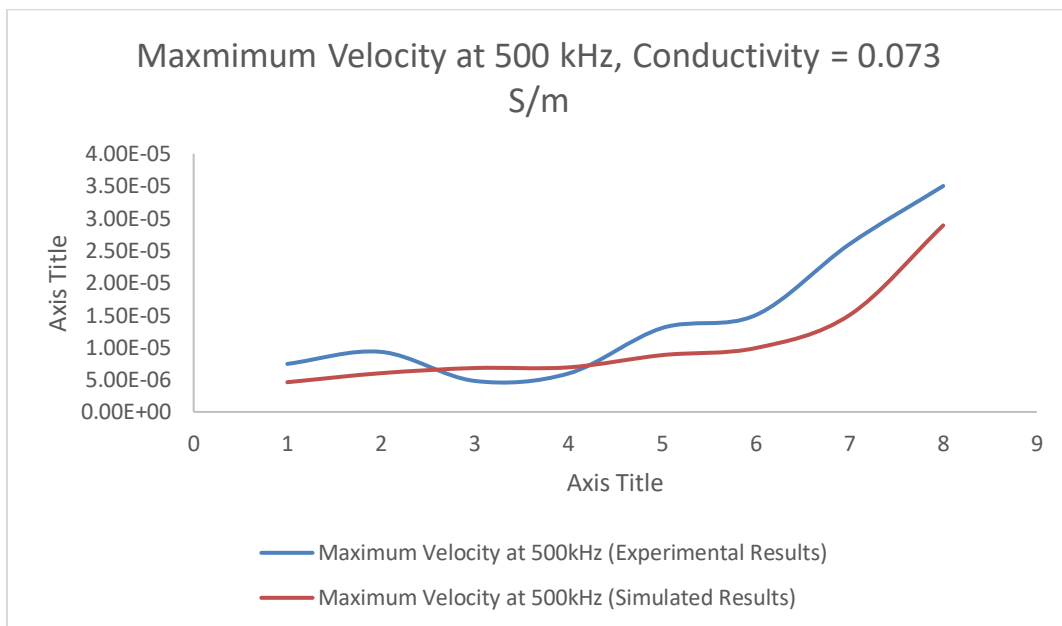


Figure 18b: Disparity between the experimental and simulated results obtained on the fluid with conductivity 0.073 S/m at 500 kHz and different voltage levels

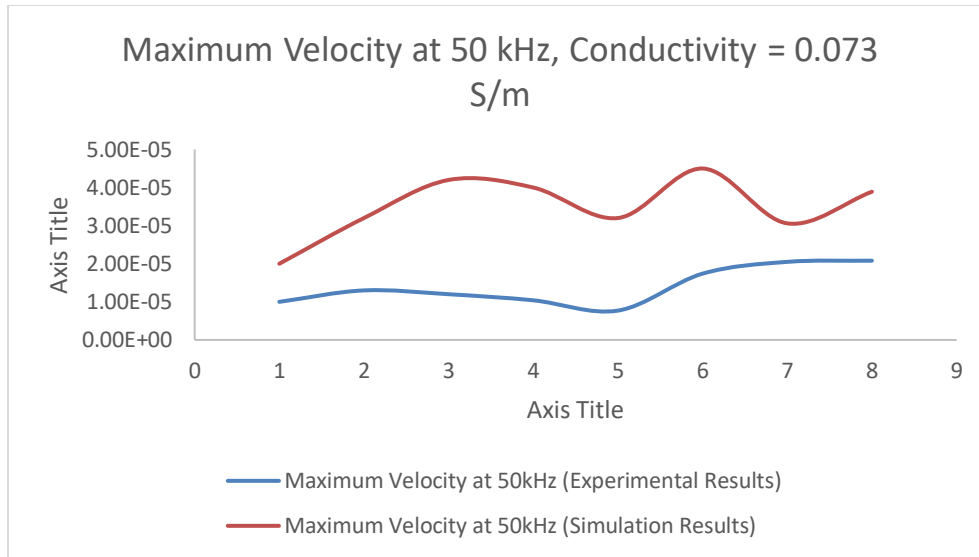


Figure 18c: Disparity between the experimental and simulated results obtained on the fluid with conductivity 0.073 S/m at 50 kHz and different voltage levels

The experimental results appear to agree with the high conductivity fluid with minimum discrepancy but, for the fluid conductivity 0.073 S/m especially at 50 kHz (Figure 18c) the experimental result variation is high due to the unknown factors. This behavior is not yet well understood, which may be caused due to experimental variations. It could also be the result of an undetermined transient thermal effect. At present we could find the exact factor that is responsible for this behavior.

5.2.2 Micromixing efficiency:

One of most common method to judge a micromixing structure is visualization of flow through dilution-type experiments. In this research, passive mixing was observed by suspending red colored dye into the fluids with conductivities 1.632 S/m and 0.073 S/m through colloidal suspension method. The normal diffusion mixing time between the dye and the buffer solution was found to be ~3 minutes. With the application of AC voltage, the mixing time was reduced to ~31 seconds and ~46 Seconds with fluid conductivities 1.632 S/m and 0.073 S/m respectively.

Therefore, micromixing through the demonstrated device was 3-5 times faster than the normal diffusion process. Also, the rate of diffusion depends on the conductivity of the buffer solution or fluid indicating faster diffusion rates.

CHAPTER VI

CONCLUSION AND FUTURE SCOPE

In these experiments, it is shown how orthogonal electrode pattern can be optimized and used as a multifunctional system. Like many other research groups flow reversal has been observed which can act as a valve to control the fluid flow. Systematic fabrication of orthogonal electrodes with proper sealing and chamber space can be used to build chips and Lab-on-Chip devices. As the orthogonal electrode pair showed potential for pumping a conventional mechanical pump can be replaced with ACEK driven components for integration into lab-on-a-chip applications. Improvement of micropump surface hydrophobicity and optimizing the multifunctionality characteristics may yield faster and efficient pumping rates.

Micromixer as a circular electrode patterned device was proposed to attain faster diffusion process. Despite of the discrepancies between the experimental and numerical results, the proposed device showed promising results by effective micromixing achieving 3-5 times faster diffusion rates compared to the normal diffusion process. The resulting performance can be used in the point of care devices having LOC for better precision and stabilized micromixing. Further investigation is being carried out to determine the capability of the proposed device as a multifunctional system.

REFERENCES

- 1) M.W. Ashraf, S. Tayyaba, and N. Afzulpurkar, "Micro Electromechanical Systems (MEMS) Based Microfluidic Devices for Biomedical Applications" *Int. J. Mol. Sci.*, 12 (2011) 3648
- 2) C. Zhang, D. and Xing, Y. Li, "Micropumps, microvalves, and micromixers within PCR microfluidic chips: Advances and trends" *Biotechnology. adv.*, 25 (2007) 483
- 3) Y. Song, T.S, and Zhao, J. "Modelling and test of a thermally-driven phase-change nonmechanical micropump" *Micromechanics and Microengineering.*,11 (2001) 713
- 4) Y. Ai, S.E. Yalcin, D. Gu, O. Baysal, H. Baumgart, S. Qian and A. Beskok, J. "A low-voltage nano-porous electroosmotic pump" *colloid interface. science*, 350 (2010) 465
- 5) N. Islam, A. Zaman, and J. Wu, "Feedback Control Circuit for Biased AC Electroosmosis Pump" *IEEE Int. Conference*, (2008) 27
- 6) P. Wang, Z. Chen, and H.C. Chang, "A new electro-osmotic pump based on silica monoliths" *Sensor and Actuators. B: Chemical.*, 113 (2006) 50
- 7) H.A. Rouabah, B.Y. Park, R.B. Zaouk, H. Morgan, M.J. Madou, and N.G. Green, "Design and fabrication of an ac-electro-osmosis micropump with 3D high-aspect-ratio electrodes using only SU-8" *Journal of Micromechanics and Microengineering*, 21 (2011) 035018
- 8) E. Kjeang, N. Djilali, and D. Sinton, "Microfluidic cells: A review" *Journal of Power Sources*,186(2009)35
- 9) Y. Yoshimi, K. Shinoda, M. Mishima, K. Nakao, and K. Munekane, "Development of an artificial synapse using an electrochemical micropump" *Journal of Artificial Organs*, 7 (2004) 210
- 10) W.Y. Sim, H.J. Yoon, O.C. Jeong, S.S. Yang, "A phase-change type micropump with aluminum flap valves" *Journal of Micromechanics and Microengineering*, 13 (2003) 286

- 11) F.J. Hong, J. Cao and P. Cheng “A parametric study of AC electrothermal flow in microchannels with asymmetrical interdigitated electrodes”. *International Communications in Heat and Mass Transfer* 38 (2011) 275–279
- 12) Marin Sigurdson, Dazhi Wang and Carl D. Meinhart “Electrothermal stirring for heterogeneous immunoassays”. *Lab Chip*, 2005, 5, 1366-1373
- 13) Jie Wu, Meng Lian, and Kai Yang “Micropumping of biofluids by alternating current electrothermal effects”. *APPLIED PHYSICS LETTERS* 90, 234103 (200)
- 14) M. Lian, N. Islam and J. Wu “AC electrothermal manipulation of conductive fluids and particles for lab-chip applications” *IET Nanobiotechnol.*, 2007, 1, (3), pp. 36–43
- 15) Wee Yang Ng, Antonio Ramos, Yee Cheong Lam, I. Putu Mahendra Wijayaad and Isabel Rodriguez “DC-biased AC-electrokinetics: a conductivity gradient driven fluid flow”. *Lab Chip*, 2011, 11, 4241–4247
- 16) Stuart J. Williams and Nicolas G. Green “Electrothermal pumping with interdigitated electrodes and resistive heaters”. *Electrophoresis* 2015, 36, 1681–1689
- 17) Quan Yua and Jie Wu “Thermally biased AC electrokinetic pumping effect for Lab-on-a-chip based delivery of biofluids”. *Biomed Microdevices* (2013) 15:125–133
- 18) Reza Hadjiaghaie Vafaie, Habib Badri Ghavifekr, Harald Van Lintel, Juergen Brugger and Philippe Renaud “Bi-directional ACET micropump for on-chip biological applications”. *Electrophoresis* 2016, 37, 719–726
- 19) J. Deval, P. Tabeling and Chih-Ming Ho “A dielectrophoretic chaotic mixer”. *Technical Digest. MEMS 2002 IEEE International Conference. Fifteenth IEEE International Conference on Micro Electro Mechanical Systems. Vol 1 P:36-39*
- 20) Yi-Kuen Lee, J. Deval; P. Tabeling and Chih-Ming Ho “chaotic mixing in electrokinetically and pressure driven micro flows”. *Technical Digest. MEMS 2001. 14th IEEE International Conference on Micro Electro Mechanical Systems. Vol 1 P:483-486*
- 21) Pablo Garcia-Sanchez, Antonio Ramos and Frieder Mugele “Electrothermally driven flows in ac electrowetting”. *Physical Review E* 81, 01503
- 22) Gunda, N. S. K. and Mitra, S. K. “Modeling of dielectrophoresis for myoglobin molecules in a microchannel with parallel electrodes”. *Proceedings of the ASME, IMECE 2009-10765 p: 463-468.*
- 23) Marin Sigurdson, Dazhi Wang and Carl D. Meinhart “Electrothermal stirring for heterogeneous immunoassays”. *Lab Chip*, 2005, 5, 1366-1373

- 24) Hope C. Feldman, Marin Sigurdson and Carl D. Meinhart “AC electrothermal enhancement of heterogeneous assays in microfluidics”. *Lab Chip*, 2007, 7, 1553–1559
- 25) Feng J. J.; Krishnamoorthy S.; Sundaram S.; “Numerical and analytical studies of electrothermally induced flow and its application for mixing and cleaning in microfluidic systems,” *Proceedings of 2004 NSTI Nanotechnology Conference and Trade Show - NSTI Nanotech 2004*. Vol 2. P:450-453
- 26) Naoki Sasaki, Takehiko Kitamori and Haeng-Boo Kim “Fluid mixing using AC electrothermal flow on meandering electrodes in a microchannel”. *Electrophoresis* 2012, 33, 2668–2673
- 27) Naga Siva Kumar Gunda, Subir Bhattacharjee, and Sushanta K. Mitra “Study on the use of dielectrophoresis and electrothermal forces to produce on-chip micromixers and microconcentrators”. *Biomicrofluidics* 6, 034118 (2012)
- 28) Alinaghi Salari and Colin Dalton “A novel ac electrothermal micropump for biofluid transport using circular interdigitated microelectrode array” *Proc. of SPIE Vol.* 9320, 932016
- 29) Khoshmanesh, K.; Nahavandi, S.; Baratchi, S.; Mitchell, A.; Kalantar-Zadeh, K. Dielectrophoretic platforms for bio-microfluidic systems. *Biosens. Bioelectron.* 2011, 26, 1800–1814
- 30) Bousse, L.; Cohen, C.; Nikiforov, T.; Chow, A.; Kopf-Sill, A.R.; Dubrow, R.; Parce, J.W. Electrokinetically controlled microfluidic analysis systems. *Annu. Rev. Biophys. Biomol. Struct.* 2000, 29, 155–181
- 31) Pohl, H.A. The motion and precipitation of suspensoids in divergent electric fields. *J Appl. Phys.* 1951, 22, 869–871
- 32) Hughes, M.P.; Morgan, H.; Rixon, F.J.; Burt, J.P.; Pethig, R. Manipulation of herpes simplex virus type 1 by dielectrophoresis. *Biochim. Biophys. Acta* 1998, 1425, 119–126
- 33) Nakano, A.; Ros, A. Protein dielectrophoresis: Advances, challenges and applications. *Electrophoresis* 2013, 34, 1085–1096
- 34) Hamada, R.; Takayama, H.; Shonishi, Y.; Mao, L.; Nakano, M.; Suehiro, J. A rapid bacteria detection technique utilizing impedance measurement combined with positive and negative dielectrophoresis. *Sens. Actuators B Chem.* 2013, 181, 439–445
- 35) Martinez-Duarte, R.; Camacho-Alanis, F.; Renaud, P.; Ros, A. Dielectrophoresis of lambda-DNA using 3D carbon electrodes. *Electrophoresis* 2013, 34, 1113–1122

- 36) Koklu, M.; Park, S.; Pillai, S.D.; Beskok, A. Negative dielectrophoretic capture of bacterial spores in food matrices. *Biomicrofluidics* 2010, 4, doi:10.1063/1.3479998
- 37) Song, Y.; Yang, J.; Shi, X.; Jiang, H.; Wu, Y.; Peng, R.; Wang, Q.; Gong, N.; Pan, X.; Sun, Y. DC dielectrophoresis separation of marine algae and particles in a microfluidic chip. *Sci. China Chem.* 2012, 55, 1–7
- 38) Menachery, A.; Kremer, C.; Wong, P.E.; Carlsson, A.; Neale, S.L.; Barrett, M.P.; Cooper, J.M. Counterflow dielectrophoresis for trypanosome enrichment and detection in blood. *Sci. Rep.* 2012, 2, doi:10.1038/srep00775
- 39) Yunus, N.A.M.; Nili, H.; Green, N.G. Continuous separation of colloidal particles using dielectrophoresis. *Electrophoresis* 2013, 34, 969–978
- 40) Young, C.-W.; Hsieh, J.-L.; Ay, C. Development of an Integrated Chip for Automatic Tracking and Positioning Manipulation for Single Cell Lysis. *Sensors* 2012, 12, 2400–2413.
- 41) Patel, S.; Showers, D.; Vedantam, P.; Tzeng, T.-R.; Qian, S.; Xuan, X. Microfluidic separation of live and dead yeast cells using reservoir-based dielectrophoresis. *Biomicrofluidics* 2012, 6, doi:10.1063/1.4732800
- 42) Jaber, F.T.; Labeed, F.H.; Hughes, M.P. Action potential recording from dielectrophoretically positioned neurons inside micro-wells of a planar microelectrode array. *J. Neurosci. Methods* 2009, 182, 225–235
- 43) Imasato, H.; Yamakawa, T. Separation of leukemia cells from blood by employing dielectrophoresis. In *Proceedings of the World Automation Congress (WAC)*, Kobe, Japan, 19–23 September 2010.
- 44) Piacentini, N.; Mernier, G.; Tornay, R.; Renaud, P. Separation of platelets from other blood cells in continuous-flow by dielectrophoresis field-flow-fractionation. *Biomicrofluidics* 2011, 5, doi:10.1063/1.3640045
- 45) Chuang, C.-H.; Huang, Y.-W.; Wu, Y.-T. System-level biochip for impedance sensing and programmable manipulation of bladder cancer cells. *Sensors* 2011, 11, 11021–11035
- 46) Rosales-Cruzaley, E.; Cota-Elizondo, P.; Sánchez, D.; Lapizco-Encinas, B.H. Sperm cells manipulation employing dielectrophoresis. *Bioprocess Biosyst. Eng.* 2013, 36, 1353–1362
- 47) J. C. McDonald and G. M. Whitesides, “Poly(dimethylsiloxane) as a material for fabricating microfluidic devices,” *Acc. Chem. Res.*, 35, (2002), 491–499

- 48) C.S. Effenhauser, G.J.M. Bruin, A. Paulus, M. Ehrat, *Anal. Chem.*, (1997), 69, 3451-3457
- 49) D.C. Duffy, J.C. McDonald, O.J.A. Schueller and G.M. Whitesides, *Anal. Chem.*, 70, (1998), 4974-4984
- 50) J.C. McDonald, D.C. Duffy, J.R. Anderson, D.T. Chiu, H. Wu, O.J.A. Schueller and G.M. Whitesides, *Electrophoresis*, (2000), 21, 27-40
- 51) V. Studer, A. Pépin, Y. Chen and A. Ajdari, *Microelectron. Eng.* (2002) in press
- 52) B. D. Gates and G. M. Whitesides, "Replication of vertical features smaller than 2 nm by soft lithography," *J. Am. Chem. Soc.*, 125, (2003), 14986–14987.
- 53) Q. Xu, B. T. Mayers, M. Lahav, D. V. Vezenov, and G. M. Whitesides, "Approaching zero: using fractured crystals in metrology for replica molding," *J. Am. Chem. Soc.*, 127, (2005), 854 855.
- 54) B. Grzybowski, D. Qin, R. Haag, and G. M. Whitesides, "Elastomeric optical elements with deformable surface topographies: applications to force measurements, tunable light transmission and light focusing," *Sens. Actuators, A*, A86, (2000), 81–85.
- 55) J. L. Wilbur, R. J. Jackman, G. M. Whitesides, E. Chang, L. Lee, and M. Prentiss, "Elastomeric optics," *Chem. Mater.*, 8, (1996), 1380–1385
- 56) MIT Material: PDMS (polydimethylsiloxane)_6.777J/2.751J Material Property Database : <http://www.mit.edu/~6.777/matprops/pdms.htm>
- 57) J. N. Lee, X. Jiang, D. Ryan, and G. M. Whitesides, "Compatibility of mammalian cells on surfaces of poly(dimethylsiloxane)," *Langmuir*, 20, (2004), 11684–11691
- 58) J. N. Lee, C. Park, and G. M. Whitesides, "Solvent compatibility of poly(dimethylsiloxane)-based microfluidic devices," *Anal. Chem.*, 75, (2003), 6544–6554
- 59) A. R. Abate, D. Lee, T. Do, C. Holtze, and D. A. Weitz, "Glass coating for PDMS microfluidic channels by sol-gel methods," *Lab Chip*, 8, (2008), 516–518
- 60) G. T. Roman, T. Hlaus, K. J. Bass, T. G. Seelhammer, and C. T. Culbertson, "Solgel modified poly(dimethylsiloxane) microfluidic devices with high electroosmotic mobilities and hydrophilic channel wall characteristics," *Anal. Chem.*, 77, (2005), 1414–1422.
- 61) COMSOL Reference
https://cdn.comsol.com/documentation/5.2.1.262/IntroductionToCOMSOLMultiphysics.nl_NL.pdf

- 62) Alex M. Djerdjev, James K. Beattie, and Robert J. Hunter “An electroacoustic and high-frequency dielectric response study of stagnant layer conduction in emulsion systems” *Journal of Colloid and Interface Science* 265 56–64 2003
- 63) A. Salari, M. B. Shafii, and S. Shirani, “An experimental review on microbubble generation to be used in echo-particle image velocimetry method to determine the pipe flow velocity,” *J Fluid Eng T ASME*, vol. 135, no. March, p. 34501, 2013
- 64) Gerard H. Markx , Mark S. Talary, Ronald Pethig “Separation of viable and non-viable yeast using dielectrophoresis” *Journal of Biotechnology* vol. 32 pp. 29-37 1994

BIOGRAPHICAL SKETCH

Rakesh Guduru was born in Andhra Pradesh, India. After completing his schoolwork at Sri Chaitanya Junior College in Vijayawada in 2010, Rakesh entered Vikas college of Engineering in Vijayawada, India. During the summer of 2014, he received a Bachelor of Technology with a major in Electrical Engineering from Jawaharlal Technological University, Kakinada. During the following two years, he was employed as a Research Assistant at University of Texas Rio Grande Valley, Texas. In August 2017, he earned his Master of Science in Engineering degree from the Graduate School of The University of Texas Rio Grande Valley. For further information please email the author at pingrakesh@hotmail.com.